Localized Mechanical Compression as a Technique for the Modification of Biological Tissue Optical Properties

Alondra Izquierdo-Román

Thesis submitted to the faculty of the Virginia Polytechnic Institute and State University in partial fulfillment of the requirements for the degree of

Master of Science

In

Biomedical Engineering

Christopher G. Rylander
John L. Robertson
Ge Wang

August 11th, 2011
Blacksburg, VA

Keywords: Compression, Mechanical Loading, Diffuse Reflectance Spectroscopy, Contrast, Resolution, Biological Tissue

Localized Mechanical Compression as a Technique for the Modification of Biological Tissue Optical Properties

Alondra Izquierdo-Román

Abstract

Tissue optical clearing aims to increase the penetration depth of near-collimated light in biological tissue to enhance optical diagnostic, therapeutic, and cosmetic procedures. Previous studies have shown the effects of chemical optical clearing on tissue optical properties. Drawbacks associated with chemical clearing include the introduction of potentially toxic exogenous chemicals into the tissue, poor site targeting, as well as slow transport of the chemicals through tissue. Thus, alternative clearing methods have been investigated. Mechanical compression is one such alternative tissue optical clearing technique. The mechanisms of action of mechanical compression may be similar to those of chemical clearing, though they have yet to be investigated systematically. This research describes the design and execution of a number of procedures useful for the quantification of the tissue optical clearing effects of localized mechanical compression. The first experimental chapter presents the effects of compression on image resolution and contrast of a target imaged through *ex vivo* biological tissue. It was found that mechanical optical clearing allowed recovery of smaller targets at higher contrast sensitivity when compared to chemical clearing. Also, thickness-independent tissue clearing effects were observed. In the second experimental chapter, dynamic changes in tissue optical properties, namely scattering and absorption coefficients (μ_s' and μ_a, respectively) were monitored during a controlled compression protocol using different indentation geometries. A reduction in μ_s' and μ_a was evident for all indentation geometries, with greater changes occurring with smaller surface area. Results indicate that localized mechanical compression may be harnessed as a minimally-invasive tissue optical clearing technique.

.

Author's Acknowledgements

First and foremost, I would like to thank my advisor, Dr. Chris Rylander, for introducing me to the topic of tissue optics and all the exciting research that is being performed in this niche field. I am grateful for all the technical guidance and support you have given me over the past two years (and then some). I would also like to thank Dr. Ge Wang and Dr. John Robertson (Dr. Bob) for serving on my M.S. committee. Dr. Bob, I would like to thank you especially for our seemingly endless supply of excised animal tissue, in all sizes, shapes, and forms.

My sincerest thanks to all my lab mates who, in one way or another, made my journey at Virginia Tech a gratifying experience. Abhijit Gurjarpadhye, Alpaslan Kosoglu, Bill Vogt, Kristen Zimmermann, Lyle Hood, and Ye Chen – thanks for all the think tank sessions, laughter breaks, for your help around the lab, and for getting pork belly at Oasis. Above all, thank you for your invaluable friendship. I would also like to thank the undergraduate students who allowed me to test my mentoring chops and contributed to my research endeavors: you all taught me more about being a good mentor than anything I could ever instill upon you. Rudy Andriani, Stephen Chang, and Leeanna Hyacinth – thank you, and I wish you the best on your own journeys. To my water polo teammates, especially Erin Weiner and Rory Brannan – thanks for teaching me the importance of balance between research and life and for coaxing me to go out and mingle with good people. Hokie Polo with a diphthong!

Geoff and Jess – without you, none of this would have been possible. I am blessed to have such absolutely amazing people in my life. You have been a tremendous support, and I owe you everything. Finally, Bella – thanks for all the entertainment, the company, the love, warmth, and stress relief. With you, everything is alright in the world.

I dedicate this thesis to my family, their undying support, encouragement, and faith in me.

Mami, Papi, Julito, Samuel, y Opie – gracias por todo el apoyo, el amor, las bendiciones y por creer en mi siempre. Me hacen falta y los quiero mucho, mucho, mucho.

Table of Contents

List of Figures

List of Tables

Chapter 1: Introduction & Overview of Research

1.1 Motivation for Current Work

The effectiveness of photothermal therapeutics, optical diagnostics, and light-based cosmetic applications is limited by their lack of ability to deliver optical radiation deep into native biological tissue. Some applications affected by this limitation include cancer ablation, photodynamic therapy, tissue imaging, port wine stain treatment, tattoo removal, scar revisions, laser hair removal, and many more. Near-collimated light is only able to penetrate a few millimeters in biological tissue due to the highly scattering nature of this material. The optical properties of biological tissue were once considered to be fixed. However, much research is being performed in the area of "tissue optical clearing" in order to develop minimally-invasive, reversible methods of altering tissue properties using a controlled and precise approach. This introduction briefly covers the basics of tissue optics and the development of tissue optical clearing strategies, including an overview of tissue optical properties, biological tissue structure, tissue optical clearing methods and mechanisms of action, as well as a discussion of prototypical devices that have been developed to achieve tissue optical clearing.

1.2 Tissue optics

1.2.1 Skin structure

Skin is the largest organ in the human body and is involved in many complex, protective functions. Skin acts to protect the body from external physical trauma, infection, as well as environmental hazards [1]. Though the mechanical attributes of skin vary depending on its location in the body, its basic composition is similar. Skin is composed of three main layers: the epidermis, dermis, and the subcutis. The epidermis is the topmost layer and is the first line of protection against surroundings, serving mainly to prevent the body from excessive water loss to the environment. The main constituents of the epidermis are melanin granules, keratinocytes, and melanocytes, allotting this tissue a thickness of about 0.07 mm to 0.12 mm [2]. The second main layer, the dermis, may be divided into two main layers: the papillary dermis and the reticular dermis. All in all, the dermis contains sweat and sebaceous glands, hair follicles, microvasculature, nervous tissue, and extracellular matrix. The extracellular matrix confers skin its structural integrity, consisting of collagen, elastin, water, and complex sugars. Although both sublayers of the dermis contain collagen fibers, the collagen in the papillary dermis is very

loosely packed and unstructured while the collagen fibers in the reticular dermis are thicker and tightly packed. Average total dermal thickness varies between 0.3 mm and 3.0 mm. Finally, the subcutis is composed mainly of fat, providing the body with necessary insulation against the elements. Although skin's complex composition is successful in acting as a protective barrier, it hinders the success of light-based diagnostic, therapeutic, and cosmetic procedures by limiting the penetration depth of light. Much research has been devoted to overcoming these limitations by altering tissue optical properties.

1.2.2 Tissue Turbidity

The numerous and complex structures composing biological tissue contribute to the problem of tissue turbidity. Tissue turbidity, in turn, leads to the attenuation of light and limited penetration depth in tissue. Light attenuation occurs due to numerous photon scattering and absorption events. Light scattering is the dominant attenuation mechanism in skin; there are approximately twenty more scattering events occurring per unit length in skin compared to absorption events [3]. Thus, skin is a highly turbid medium in the visible to near-infrared wavelength range. Scattering events in tissue are due to differences in the optical index of refraction, n, of the individual constituents. All the different constituents of skin, mentioned in the previous section, have slightly different indices of refraction. The main contributor to light scattering in tissue is water due to the high index of refraction mismatch (Δn) between it and the rest of the proteinaceous constituents. Water accounts for ~70% of the total weight of skin while collagen accounts for ~75% of the dry weight of skin [4]. Their respective indices of refraction are n = 1.33 for water and n = 1.43-1.53 for collagen [5]. The direction and intensity of scattered light is a function of the shape and size of the scattering particles, giving rise to both Rayleigh and Mie scattering [6, 7].

1.2.3 Optical properties

Absorption, scattering, specular reflection, and diffuse reflection are all different types of light-tissue interactions that are affected by tissue optical properties. These light-tissue interactions are illustrated in Figure 1-1.

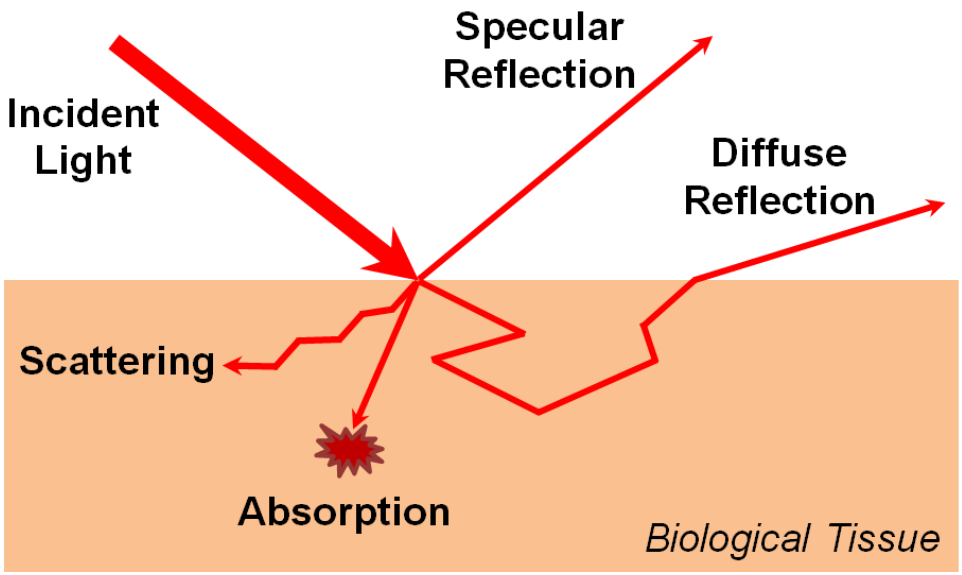

Figure 1-1: Schematic representation of light-tissue interactions.

Tissue optical properties also affect the penetration depth of light in tissue. These include: refractive index, scattering and absorption coefficients, and direction of scattering. Penetration depth, δ, is inversely proportional to the scattering and absorption coefficients (μ_s and μ_a), seen in Equation (1.1) below.

$$\delta = \frac{1}{\mu_s + \mu_a} \tag{1.1}$$

Refractive index is a measure of how much a medium slows down the speed of a photon when it comes into contact with the medium, seen in Equation (1.2) below,

$$n = \frac{c}{v_p} \tag{1.2}$$

where c represents the speed of light through a vacuum and v_p represents the phase velocity of a particular wavelength of light in a medium. Due to the numerous constituents with dissimilar indices of refraction in tissue, the velocity of a photon traveling through tissue will change amplitude at all interfaces. It is this variation in refractive index that impels a scattering event.

Since the differences in refractive index between water and other tissue constituents gives

rise to scattering and absorption events, it may follow naturally that modifying the water concentration in tissue will alter the optical properties locally. Altering optical properties will affect the local fluence in tissue when a light is incident on the tissue. Fluence refers to the amount of energy delivered per unit area and is defined by Equation (1.3) below,

$$\Phi(z) = \Phi_o e^{-\mu_{eff} z} \tag{1.3}$$

where Φ_o is the irradiance on the tissue surface, z is the penetration depth of light into the tissue, and μ_{eff} is the effective attenuation coefficient. As described previously, light attenuation is influenced by both the scattering and absorption events occurring in the tissue. The effective attenuation coefficient is defined in Equation (1.4) below,

$$\mu_{eff} = \sqrt{3\mu_a(\mu_a + \mu_s')} \tag{1.4}$$

where μ_s' is the reduced scattering coefficient and μ_a is the absorption coefficient.

1.2.4 Tissue Optical Clearing

Tissue optical clearing is a technique used to reversibly modify the optical properties of biological tissue in a controlled, precise manner, allowing the delivery of focused light deeper into tissue. In terms of therapeutics, this may allow more precise targeting of tumor tissue, for example, during photothermal treatment without damaging adjacent healthy tissue. In terms of imaging and diagnostics, tissue optical clearing may increase the imaging depth and resolution of optical coherence tomography (OCT), confocal endoscopy, and bioluminescence tomography [8-11].

1.2.4.1 Chemical Tissue Optical Clearing

Current research investigating tissue optical clearing centers on the delivery of exogenous chemicals, hyperosmotic agents, to increase optical clarity and reduce scattering [12-20]. Researchers have proposed three mechanisms governing the reduction in light scattering due to the introduction of hyperosmotic agents: first, dehydration of the tissue; second, replacement of

water with the hyperosmotic agents, which better match the refractive index of proteins; and finally, the dissociation of collagen fibers. These, and other potential mechanisms, may explain the clearing of tissue with observed differences based on the tissue type, chemical used, and application method. There are, however some drawbacks to chemical tissue optical clearing methods. Chemical clearing is a slow process requiring the transport of the agent through the tissue. Additionally, this method has the potential for toxicity, as an exogenous agent is introduced into the body. Chemical clearing is an invasive procedure, which interferes with the *stratum corneum*'s protective barrier function. Finally, chemical clearing does not allow specific targeting or selectivity.

1.2.4.2 Mechanical Tissue Optical Clearing

Since dehydration has been identified as a possible mechanism of action of tissue optical clearing, research groups hypothesized that tissue dehydration using non-chemical techniques may afford the same optical clearing benefits as chemical clearing techniques, but with fewer drawbacks [21]. A non-chemical alternative would be less invasive and potentially safer, providing faster, localized, more repeatable optical clearing results. Localized mechanical compression has been identified as one such method for non-chemical tissue optical clearing. Localized mechanical compression is thought to induce local dehydration through water removal from tissue. The application of a mechanical force on tissue is believed to result in the lateral expulsion of water out of the zone of compression. This modification in water content, as well as the change in tissue thickness at the site, is believed to alter optical properties of the tissue at the compressed region. Figure 1-2 portrays the proposed mechanisms occurring due to the introduction of a mechanical force on tissue.

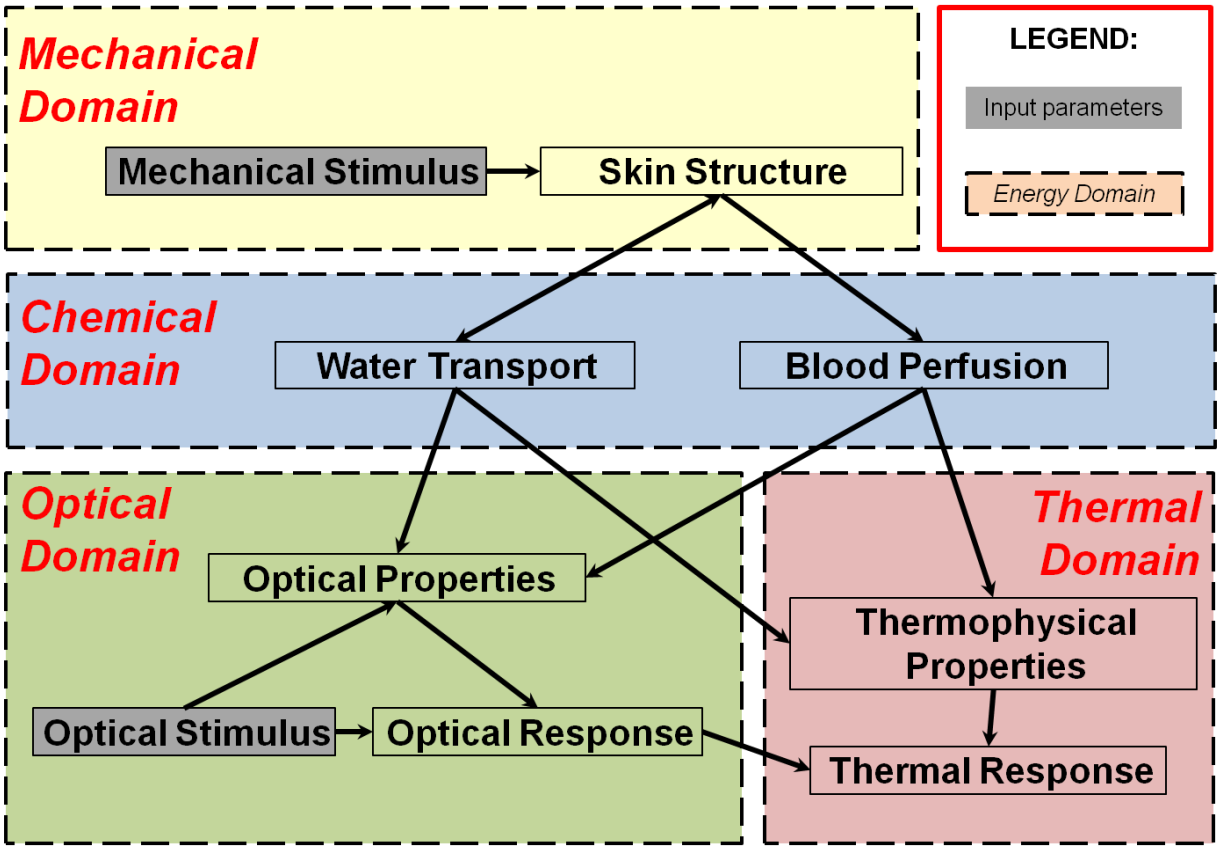

Figure 1-2: Hypothesized mechanisms of action of mechanical optical clearing [22].

Localized mechanical compression results in a cascade of coupled effects across mechanical, chemical, optical, and thermal domains. A mechanical stimulus, in this case localized mechanical compression, alters the skin structure, which leads to a change in the local blood perfusion as well as the water transport within the tissue. These last two effects result in modification of the tissue's thermophysical and optical properties.

1.2.4.3 Tissue Optical Clearing Devices

Tissue optical clearing devices, seen in Figure 1-3, are an embodiment of this mechanical tissue optical clearing technique. Rylander, *et al.*, and Drew, *et al.*, have designed and tested several device prototypes consisting of an array of hemispherical pins with a circumscribing brim [21, 23]. The devices deliver localized compression using a 750 mm Hg vacuum pressure source. These devices interface with the skin surface and form a relatively airtight seal when a vacuum is actuated. This causes the skin to be drawn up in between the pins, resulting in a reactive downwards force with the pins compressing the tissue underneath.

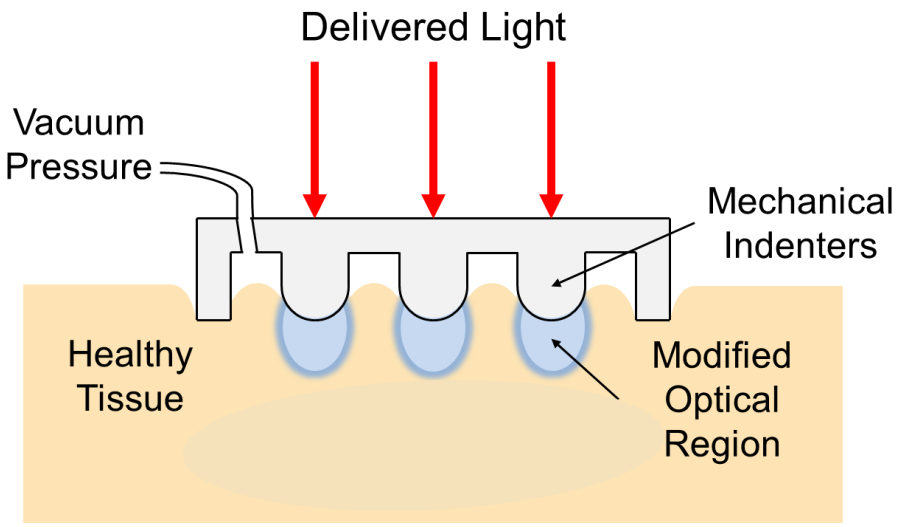

Figure 1-3: Schematic of prototypical tissue optical clearing device.

In vivo application of these tissue optical clearing device prototypes resulted in reddening in the regions in between the pins and in darkening directly underneath the pins, Figure 1-4a. The reddening was hypothesized to be due to the pooling of blood that had been displaced out of regions beneath the pins while the darkening under the pins potentially indicated the modification of optical properties. After the device was removed from the tissue, the skin rebounded to normal thickness and the areas of discoloration disappeared. Light transmission experiments through *ex vivo* porcine skin were also performed, using white light photography. *Ex vivo* porcine skin specimens, ~3 mm thick, were compressed using the tissue optical clearing device prototypes. After compression, epidermal and dermal pictures of the skin revealed increased light transmission through regions that had been compressed, seen in Figure 1-4b [21].

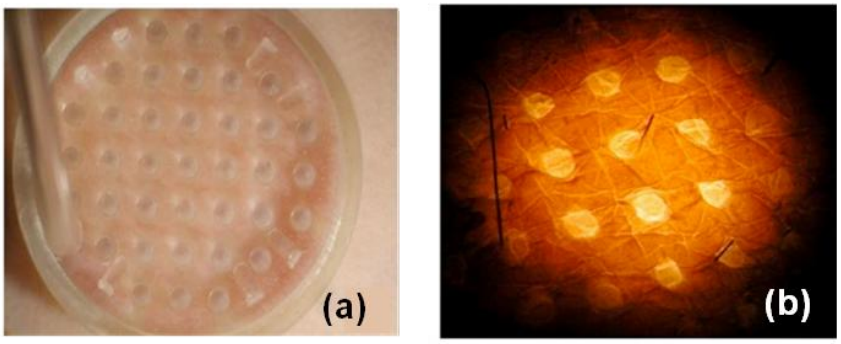

Figure 1-4: (a) TOCD on human skin, (b) Transilluminated porcine skin after TOCD application [21].

1.3 **Problem Statement and Scope of Thesis**

The applications and mechanisms of action of localized compression as a tissue optical clearing technique have not been fully explored. This thesis describes the effects of localized mechanical compression related to the modification of tissue optical properties. Three specific objectives are addressed in this thesis. The first objective, as described in Chapter 2, is the demonstration of enhanced image recovery through biological tissue using a minimally-invasive localized mechanical compression technique. The second objective, also addressed in Chapter 2, is a demonstration that optical clearing occurring due to mechanical compression is not solely the result of tissue thickness reduction. The final objective, addressed in Chapter 3, is to provide a quantitative assessment of the changes in tissue optical properties occurring as a result of this mechanical compression procedure. Finally, Chapter 4 summarizes the research presented in this thesis, suggests future work to be performed, and discusses potential applications of the optical clearing technique described. Implementation of this tissue clearing strategy has the potential to enhance existing optical diagnostic, therapeutic, and cosmetic procedures, as well as imaging modalities to be used at the patient's bedside and in research environments.

Chapter 2: Mechanical Tissue Optical Clearing Technique Increases Imaging Resolution and Contrast through *Ex Vivo* Porcine Skin

Alondra Izquierdo-Román[1], William C. Vogt[1], Leeanna Hyacinth[2], and Christopher G. Rylander Ph.D[1,3]

[1]School of Biomedical Engineering and Sciences
Virginia Polytechnic Institute and State University, Blacksburg, VA 24060
[2]Department of Biomedical Engineering
Columbia University, New York, NY 10027
[3]Department of Mechanical Engineering
Virginia Polytechnic Institute and State University, Blacksburg, VA 24060

Background and Objectives: Mechanical tissue optical clearing permits light delivery deeper into turbid tissue, which may improve current optical diagnostics and laser-based therapeutic techniques. We investigated the effects of localized compression on brightfield imaging through *ex vivo* porcine skin by evaluating resolution and contrast of a target positioned beneath native, mechanically compressed, or chemically cleared specimens. We also evaluated the effects of indentation on dynamic tissue thickness and light transmission.

Study Design/Methods: A 5 mm diameter, hemispherically-tipped, manual load transducer was used to compress specimens using 2-44 N for 60 seconds. Chemically cleared specimens were immersed for 1 hour in glycerol or dimethyl sulfoxide. A USAF 1951 resolution target was positioned beneath specimens and imaged using brightfield microscopy. Resolution and contrast of target features were analyzed using Rayleigh's resolution criterion and Michelson's contrast definition. In separate experiments, a mechanical test instrument was used to compress and hold specimens at a final thickness while measuring applied load and light transmission.

Results: Image intensity profiles showed that while uncompressed skin did not allow resolution of any target, localized compression allowed maximum resolution (least line width) of 173 ± 21 μm. Mechanical clearing achieved up to 4 times higher maximum resolution and 2-3 times higher contrast sensitivity than chemical immersion. Resolving capability was highly correlated with compressive tissue strain. Light transmission increased during tissue compression, but also increased while holding final thickness constant.

Conclusion: Localized compression is an effective technique for increasing resolution and contrast of target features through tissue and may improve light-based diagnostics. Thickness reduction and other mechanisms appear to contribute to this effect.

Key words: compression; USAF target; indentation; load; glycerol; thickness; brightfield

2.1 Introduction and Background

The inhomogeneous microstructure of native biological tissue is responsible for the multiple scattering of incident light. This natural tissue-light interaction hinders the effectiveness of diagnostic and therapeutic procedures, limiting the amount of energy delivered to a specific target, and even possibly damaging areas of non-targeted healthy tissue [18, 19, 24, 25]. Tissue optical clearing techniques attempt to control the optical properties of biological tissue in order to improve diagnostic and treatment protocols. Tissue optical clearing permits the delivery of near-collimated light deeper into biological tissue, which can potentially improve optical diagnostic techniques such as *in situ* confocal microscopy, optical coherence tomography (OCT), and reflectance spectroscopy [18, 23, 25, 26]. Tissue optical clearing may also improve optical therapeutic techniques such as photodynamic therapy (PDT) and laser-based cosmetic applications including hair and tattoo removal [14, 15, 21, 23].

Previous studies have investigated tissue optical clearing by delivery of hyperosmotic chemical agents, such as glucose, dimethyl sulfoxide (DMSO), and glycerol [19, 26]. Findings indicate that the success of these chemical techniques could be attributed to factors such as dehydration, refractive index matching, or the structural modification of collagen fibers [12, 14, 15, 18, 21]. Water and protein, two of the main constituents of biological tissue, contribute to light scattering due to intrinsic differences in their refractive indices. Hyperosmotic agents used in chemical-based tissue clearing may allow for increased refractive index matching between tissue constituents, reducing the amount of light scattering within tissue and increasing the amount of focused or near-collimated light delivered to a target region. A recent study suggests that chemical-based tissue clearing may be attributed to an increase in the anisotropy of scattering in addition to a decrease in scattering coefficient due to enhanced refractive index matching [16].

The displacement or removal of water in *ex vivo* skin by air dehydration (without the introduction of exogenous chemicals) has been previously shown to lead to scattering reduction [15]. Optical clearing of skin has also been achieved using localized mechanical compression, which is thought to be the result of local interstitial water displacement [15, 21, 23]. As water is displaced from local regions of high compressive mechanical stress, the concentrations of sugars and/or proteins (*i.e.*, proteoglycans) within the ground substance may increase, causing a decrease in the refractive index mismatch between aqueous ground substance and collagen

matrix. Mechanical optical clearing techniques are potentially less invasive than chemical methods since the integrity of the stratum corneum barrier is maintained and no exogenous chemicals are introduced into the tissue [14, 21].

In this study, we investigate the effects of localized mechanical compression on the delivery of light through *ex vivo* porcine skin. Resolution and contrast of a USAF 1951 transmission resolution target positioned beneath native or compressed porcine skin specimens were assessed using established imaging techniques. We also perform these experiments for skin specimens immersed in optical clearing agents, specifically glycerol and DMSO. Finally, we evaluate the dynamic effects of localized compression on light transmission through skin specimens. Tissue thickness, load, and light transmission were simultaneously measured during displacement-controlled compression. We hypothesize that localized compression will induce an increase in resolution and contrast sensitivity, as well as an increase in light transmission through the tissue. The light transmission experiment is designed to indicate whether reduced tissue thickness is the only mechanism of action, or if there are additional contributing factors such as modified optical properties.

2.2 Materials and Methods

2.2.1 Imaging Resolution and Contrast Study

2.2.1.1 Skin Specimen Preparation

Ex vivo porcine abdominal skin was obtained for experimentation from a young female pig and used within 48 hours postmortem. Porcine skin specimens were prepared by removing the adipose layer through excision, leaving only the dermal and epidermal layers of the tissue. The resulting specimens were approximately 1.96 ± 0.15 mm thick, with a thickness range between 1.60 mm and 2.22 mm. Specimens were trimmed to 2 cm x 2 cm squares to maintain consistency between experimental trials and stored at 4ºC in a phosphate buffered saline (PBS) moistened container prior to experimentation. The specimens were allowed to equilibrate to room temperature prior to compression. Before compression, each porcine skin specimen was placed between two glass slides and three thickness measurements were taken along the specimen with calipers, permitting calculation of an average thickness for each specimen.

2.2.1.2 Load Selection

The loads chosen in imaging experiments (2 N, 4, N, 22 N, and 44 N) correspond to pressures ranging between ~0.1 to ~2 MPa. Pain studies using indenters on the skin of human test subjects have reported pain tolerance values in the range of ~0.5 to ~1.1 MPa [27-30], depending on the anatomical location of the indenter. The lower end of our load range is well within the tolerable ranges presented in literature, making these loads feasible for potential clinical use. Furthermore, prototypical tissue optical clearing devices have been shown to deliver ~0.13 MPa of pressure [21], while still allowing the enhancement of light transmission through biological tissue.

2.2.1.3 Mechanical Compression

Skin specimens were compressed using a 5 mm diameter hemispherically-tipped glass rod. Load was manually applied at a constant level (2 N, 4 N, 22 N, or 44 N) for a period of 1 minute using a calibrated spring-loaded scale (Field & Stream, Minneapolis, MN). Five specimens were tested for each load condition. Specimen thickness in the center of the compressed region was determined immediately following compression using c-shaped calipers. Compressed specimens were placed above a glass slide to facilitate the thickness measurement procedure and minimize error. We define an "effective compressive tissue strain", e, which captures the relative deformation of the compressed regions of tissue specimens as

$$e = \frac{|T - T_0|}{T_0} \tag{2.1}$$

where T_0 is initial tissue thickness and T is deformed thickness.

2.2.1.4 Chemical Immersion

Skin specimens prepared as described previously were immersed in 15 mL of anhydrous glycerol (13 M) or anhydrous DMSO (14 M) for 60 minutes. Prior to imaging, each specimen was removed from the immersion agent and gently patted with a cotton swab to remove all agent from the specimen surface. For each chemical agent, five specimens were tested. Effective tissue strain due to chemical immersion was calculated in the same manner as described previously for

mechanical compression.

2.2.1.5 Imaging Technique

USAF 1951 fused silica targets are designed for the calibration of imaging systems [31]. The resolution target consists of multiple groups, each containing several elements. An element is an individual grouping of three bars of equal width, with spacing also equal to this width. In this study, a USAF 1951 3-bar transmission resolution target (Max Levy Autograph Inc., Philadelphia, PA) was placed beneath native, mechanically compressed, and chemically immersed skin specimens. USAF transmission targets allow white light to be transmitted through the translucent bars, as seen in Figure 2-1, allowing the assessment of resolution and contrast through the tissue.

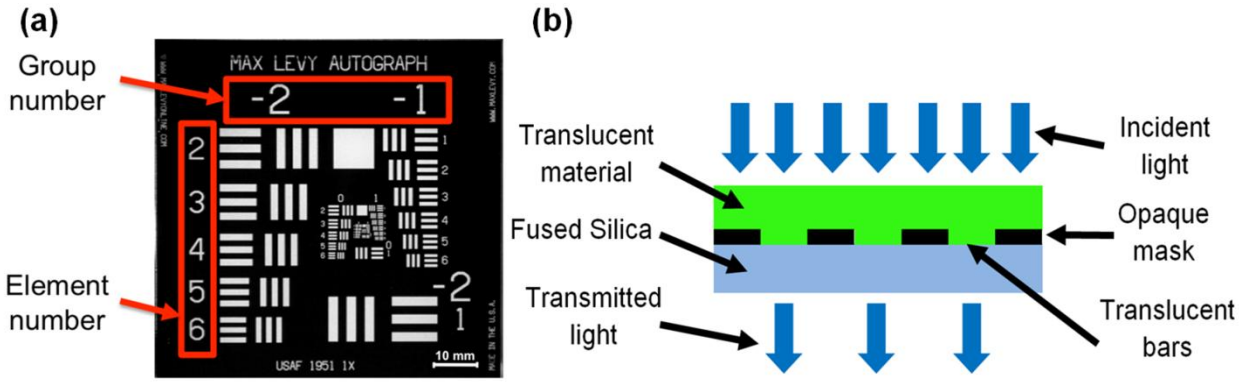

Figure 2-1: (a) Image of the USAF 1951 resolution target (3" x 3") denoting group and element numbering schemes (b) Schematic cross-sectional view of light transmission through the USAF 1951 resolution target element.

Prior to mechanical compression or chemical immersion, each specimen was placed between a glass slide and the resolution target. The glass slide, skin specimen, and target were positioned on a microscope stage permitting acquisition of a brightfield transmission image of the target at location Group -2, Element 2 (2,000 µm line width). This native (control) transmission image of the target through the skin was acquired with a Leica DM IL LED inverted microscope (Leica® Microsystems Inc., Bannockburn, IL). Light from the LED source of the microscope passed through the translucent bars of the USAF target. The unmasked white light was further transmitted through the porcine skin specimen and underlying glass slide, and collected by the

microscope objective (Figure 2-2). Following mechanical compression or chemical immersion, specimens were placed over the glass slide, and images of the resolution target element bars could were acquired. This process was repeated for target groups/elements of decreasing size, by moving the target relative to the stationary skin region. The image acquisition procedure was short (~4 minutes) and specimens did not undergo significant elastic recovery (thickness increase) during this timeframe.

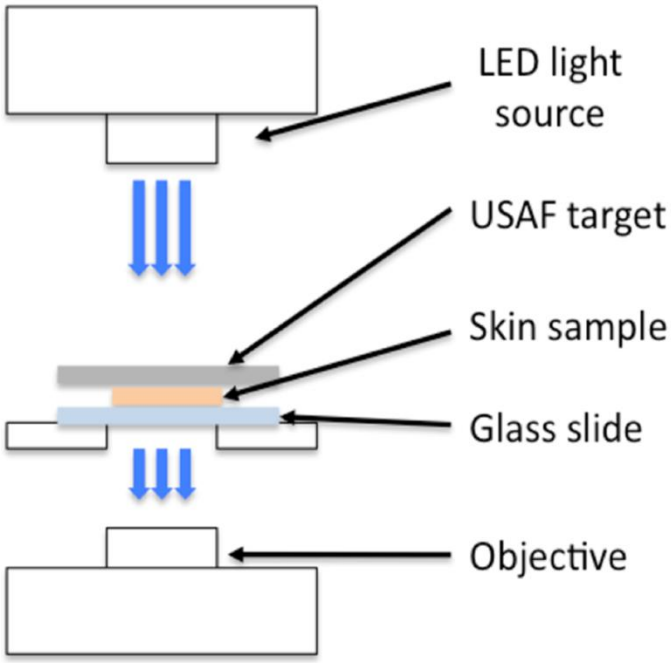

Figure 2-2: Schematic of inverted microscope setup.

2.2.1.6 Image Analysis

Brightfield transmission images were analyzed to permit comparison of the imaging resolution and contrast through native, compressed, and chemically immersed tissue specimens. Image analysis was performed using Matlab (Mathworks, Natick, MA). In order to quantitatively analyze the images, the raw color images were converted to grayscale to obtain an 8-bit intensity value (0-255) at each pixel.

A rectangular region of interest (ROI) was selected in each image using two different methods. In method 1, the ROI was selected above the entire resolution target element (containing all three bars), as shown in Figure 2-3a. In method 2, multiple ROIs were centered above single bar-space interfaces. With either method, pixel intensity values were averaged

along the length of each target bar within the selected rectangular ROI (*e.g.*, vertically along Figure 2-3a or Figure 2-3c). This yielded an averaged intensity profile across the ROI (as shown in Figure 2-3b or Figure 2-3d). Whenever possible, ROI method 1 was preferred because it captured all the target element edge data available for analysis, making it a more robust method. However, ROI method 2 was implemented for two special circumstances: first, when the area of compressed tissue was smaller than the element size (obscuring a portion of the target element bars), and second, following chemical immersion which structurally modified the specimen surface.

Resolution is the ability to visually differentiate between two adjacent objects in an image. To determine the maximum imaging resolution of the target bars beneath each skin specimen, the average intensity profile across each ROI was analyzed. Resolution was quantified by identifying the smallest bar spacing in which intensity peaks and valleys, corresponding to target bars and spaces, could be distinguished according to Rayleigh's criterion [32]. Rayleigh's criterion dictates that if the intensity of the valley region, I_{min}, is less than or equal to $8/\pi^2$ (~0.81) times the maximum intensity of the peaks, I_{max}, then the bars are resolved [33]. In the example shown in Figure 2-3b and Figure 2-3d, the bars are resolvable since I_{min} is less than the value at the red dashed line, which represents $(8/\pi^2)*I_{max}$. If ROI Method 2 was used, multiple regions within the image that appeared to show intensity peak/valley behavior (corresponding to a bar edge) were selected and submitted to Rayleigh's resolution criterion. If at least three ROIs within the entire image were resolvable, the target was said to be resolved.

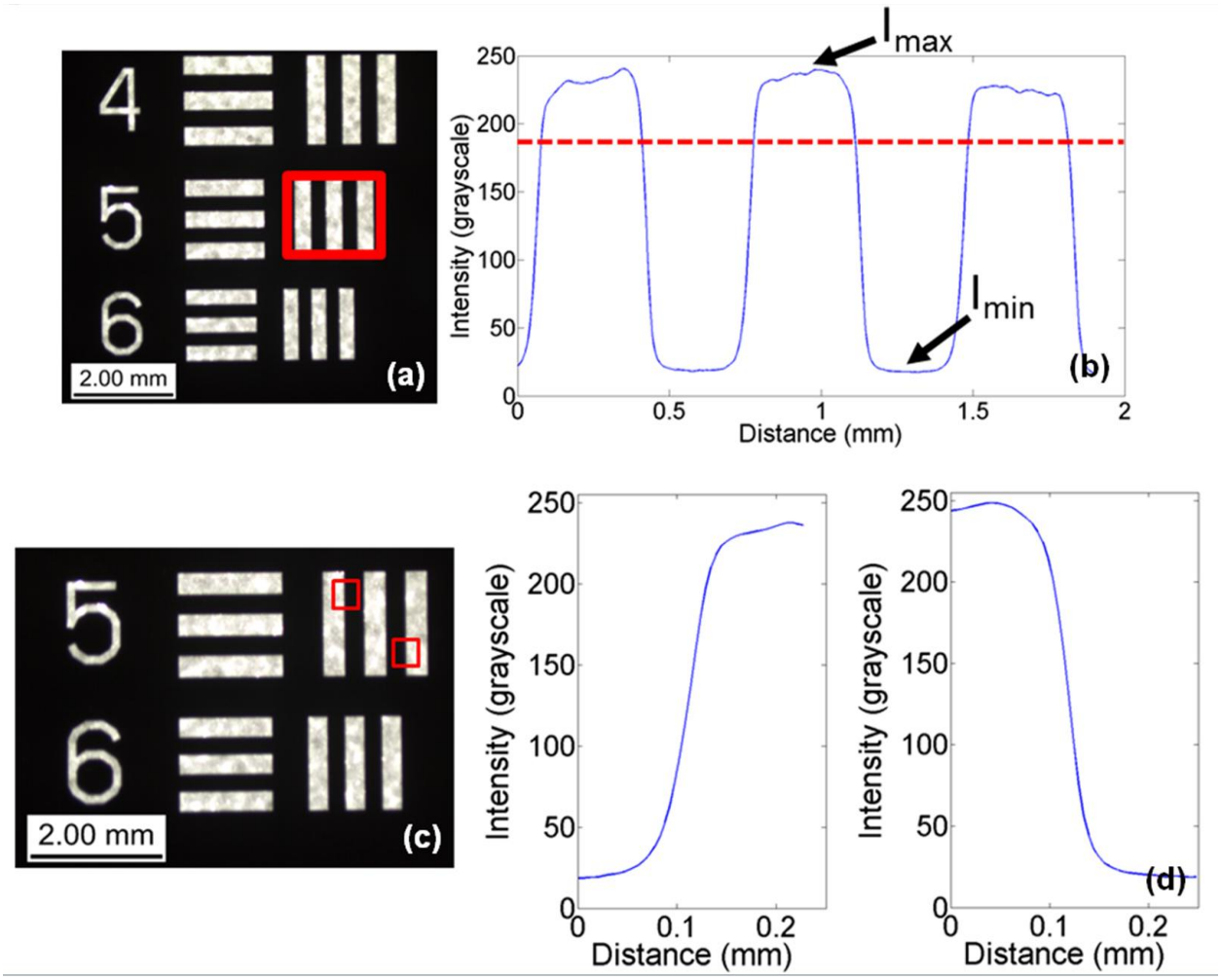

Figure 2-3: (a) Image of USAF 1951 Target, Group 0, Elements 4-6. The ROI selected in the image (red box, method 1) was used to generate the intensity profile plot. (b) Intensity profile plot. Peaks correspond to the white bars of the target ROI in (a). Valleys represent the dark spaces between the target bars. The red line denotes Rayleigh's criterion for determining resolution. (c) ROI selection method 2. (d) Intensity profile plots corresponding to the ROI's shown in (c).

Contrast sensitivity was evaluated for resolvable target bars beneath tissue specimens. Contrast sensitivity is related to the relative intensity difference between evenly spaced adjacent light and dark areas. Contrast sensitivity, *C*, is defined by Michelson as

$$C = \frac{I_{max} - I_{min}}{I_{max} + I_{min}} \times 100\% \tag{2.2}$$

where I_{max} represents the maximum intensity and I_{min} represents the minimum intensity [34, 35]. The features leading to these two intensity extrema must be adjacent in order for this relationship to be valid. For our study, I_{max} and I_{min} were determined based on the average intensity profile across each ROI as described previously.

2.2.2 Light Transmission Study

2.2.2.1 Skin Specimen Preparation

Ex vivo porcine abdominal skin was obtained and prepared as described previously for imaging experiments. The resulting specimens (N=10) were 1.44 ± 0.34 mm thick, with a thickness range between 0.85 mm and 2.00 mm. Handling, storage, and usage followed the same process detailed previously. Porcine skin specimen thickness was calculated dynamically during mechanical compression.

2.2.2.2 Experimental Setup

Using a BOSE® ElectroForce® 3100 mechanical testing instrument, tissue displacement, load, and light transmission were measured simultaneously. This instrument has a displacement resolution of 1.5 μm and a loading resolution of 6 mN with a 22 N load cell, which provides satisfactory displacement and load resolution for this study. As shown in Figure 2-4, *ex vivo* porcine skin samples were locally indented by a hemispherically-tipped transparent sapphire rod with a diameter of 3 mm. The rod was epoxy bonded to a polycarbonate housing fastened to the electromagnetic displacement cell of the ElectroForce instrument. A 670 nm laser source and a collimator delivered light to the transparent rod and the underlying tissue.

Tissue samples were placed beneath the rod on a glass sheet attached to a piece of aluminum square tubing. A 12.5 mm diameter hole in the tubing beneath the glass sheet allowed light to be transmitted through the tissue to a large-area photodetector (1 cm x 1 cm), which generated an electrical signal proportional to the light transmitted through the sample (Newport detector #818 and optical power meter #1931-C). During compression, the instantaneous optical power transmitted through the sample was recorded, allowing simultaneous dynamic measurement of

tissue thickness, load, and light transmission.

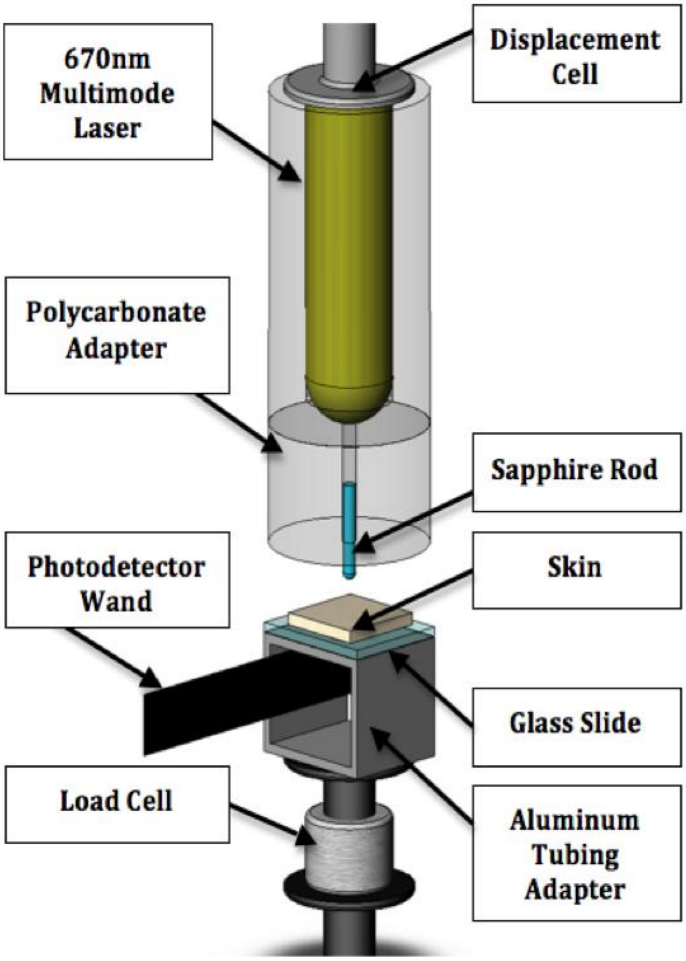

Figure 2-4: Compression experimental components. Optical power transmitted through porcine skin, applied load, and tissue thickness were recorded simultaneously.

2.2.2.3 Mechanical Compression

Transient measurement of optical power transmission through tissue during localized compression provides insight into the correlation between the effects of load and tissue thickness change on light transmission. A compression protocol was developed to evaluate light transmission during two separate compression stages: 1) displacement-controlled compression to a final tissue thickness of 0.5 mm at a displacement rate of 0.02 mm/sec (strain rate of ~10^{-2} /sec) and 2) dwell at constant tissue thickness of 0.5 mm for 120 seconds. Displacement, load, and optical power transmission were recorded with the same software at a rate of 50 Hz.

Both initial and dynamic tissue thickness were critical parameters in this mechanical compression experiment. The indenter was first brought into contact with the glass sheet and this position, x_g, was recorded. Contact was defined as the position at which the load magnitude exceeded 0.01 N. After placing the sample on the glass slide, the compression protocol was executed. The contact position of the top surface of the sample, x_c, was calculated in post-processing using the same load threshold definition, and the dynamic tissue thickness, $T(t)$, was calculated as

$$T(t) = (x_c - x_g) - x(t) \tag{2.3}$$

where $x(t)$ is the measured displacement signal at time t. Displacement-controlled deformation was chosen over load-controlled deformation in order to correlate results at the same final thickness. Given two tissue samples of different initial thicknesses, if both samples were compressed to the same final thickness, one would have a higher relative compressive strain than the other. If mechanical compression only increases light transmission by reducing tissue thickness, both samples would have the same light transmission at the same final thickness. However, if our hypothesis is correct and compression causes additional modification of optical properties, we would expect the sample that underwent more strain (and stress) to allow greater light transmission at the same final thickness.

2.3 Results

2.3.1 Imaging Resolution and Contrast Study

2.3.1.1 Mechanical Compression

Imaging through native skin specimens (*i.e.*, control, uncompressed, and unimmersed) did not allow resolution of the target bars as seen in Figure 2-5a. The image intensity profile of the target viewed through uncompressed tissue did not allow the recovery of the peaks associated with the target bars (Figure 2-5b). Figure 2-6a-b shows raw images and intensity profiles for representative resolvable target elements for selected load cases. These profiles indicate that at least one bar may be resolved according to Rayleigh's criterion. These images also demonstrate

transmission through the compressed region relative to the natural turbidity of the surrounding uncompressed tissue.

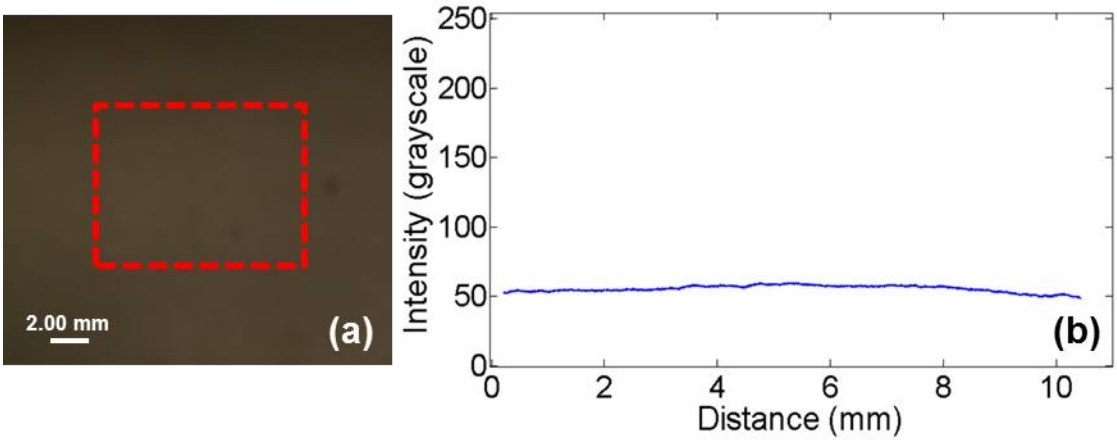

Figure 2-5: (a) Uncompressed skin specimen over target in Group 0, Element 2, corresponding to a line width of 445 µm. The dashed box represents the ROI selected for analysis. (b) Intensity plot of target under native (uncompressed) skin.

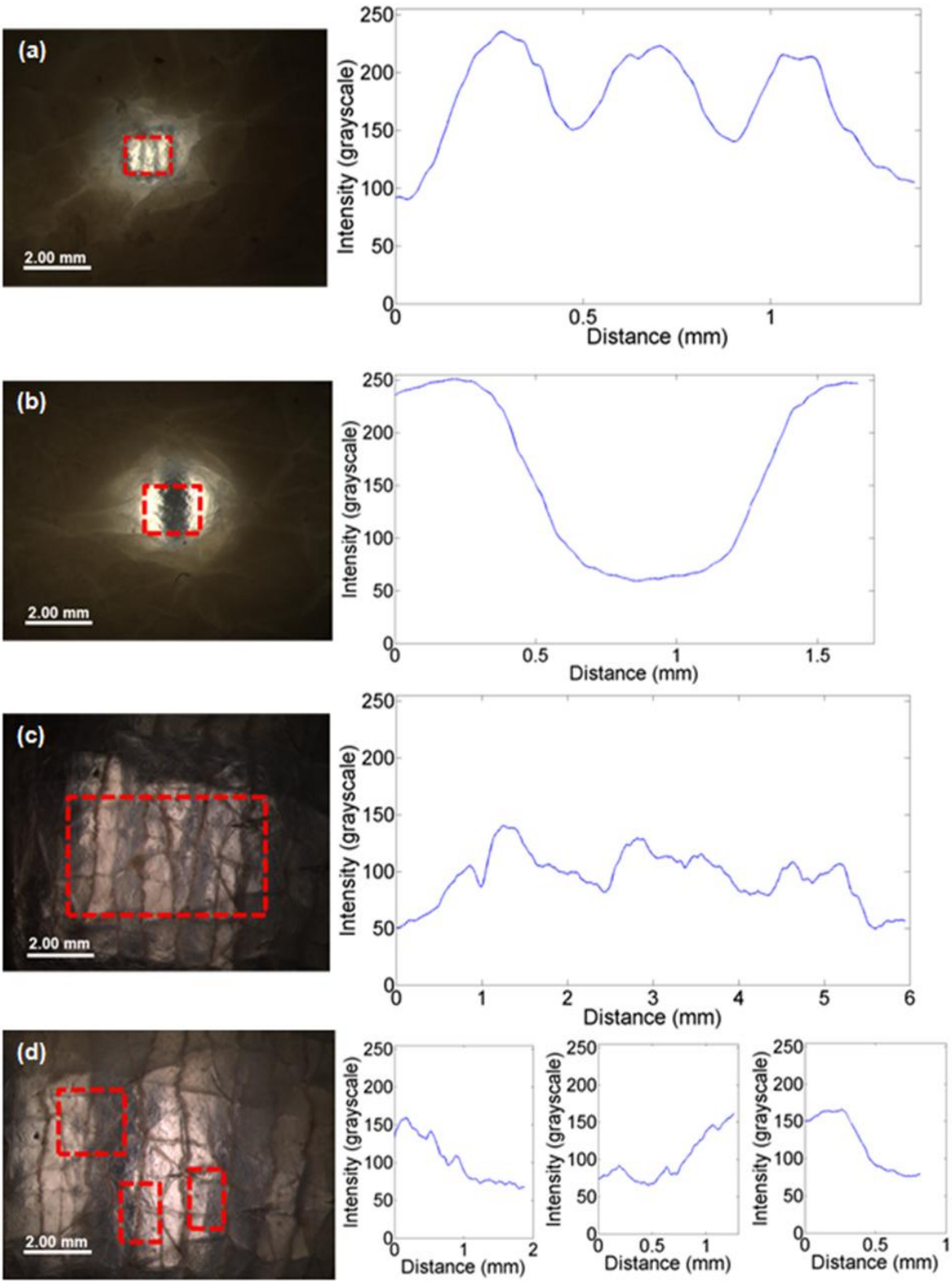

Figure 2-6: Representative images (ROI outlined in dashed boxes) and intensity plots for (a) Group 1, Element 2 following 22 N compression using ROI Method 1, (b) Group -1, Element 1 following 22 N compression using ROI Method 2, and (c) Group -1, Element 2 following

glycerol immersion using ROI Method 1, (d) Group -2, Element 2 following glycerol immersion using ROI Method 2.

The maximum resolution achieved with 2 N compression was a line width of 198 μm (Group 1, Element 3), with an associated thickness reduction equivalent to -69% strain. The maximum resolution achieved with 4 N compression was a line width of 281 μm (Group 0, Element 6), with an associated thickness reduction equivalent to -43% strain. The 22 N trials allowed resolution of a line width of 157 μm (Group 1, Element 5), with an associated thickness reduction equivalent to -75% strain. The maximum resolution achieved with 44 N compression was 250 μm (Group 1, Element 1), with an associated thickness reduction equivalent to -50% strain. Figure 2-7 shows contrast sensitivity as a function of line width for all the mechanical compression loads investigated in this study. At the highest resolution (smallest line width, ~150-250 μm), the contrast sensitivity varied between 15-25%. For line widths approaching 1.8 mm, contrast sensitivity increased to ~45-58%.

2.3.1.2 Chemical Immersion

Figure 2-6c-d shows resulting images and intensity profiles for representative resolvable target elements imaged through glycerol-immersed skin. The maximum resolution achieved with one hour of DMSO immersion was a line width of 1122 μm (Group -2, Element 6), with an associated thickness reduction equivalent to -4% strain. The maximum resolution achieved with one hour of glycerol immersion was a line width of 794 μm (Group -1, Element 3), with an associated thickness reduction equivalent to -2% strain. Figure 2-7 shows contrast sensitivity as a function of line width for both glycerol and DMSO immersed specimens. At the highest resolution, the contrast sensitivity ranged from ~10 to 15%. For greater line widths, those approaching 1.8 mm, contrast sensitivity increased to ~15-23%. Standard error was ~20-35% of the mean contrast sensitivity for all clearing techniques.

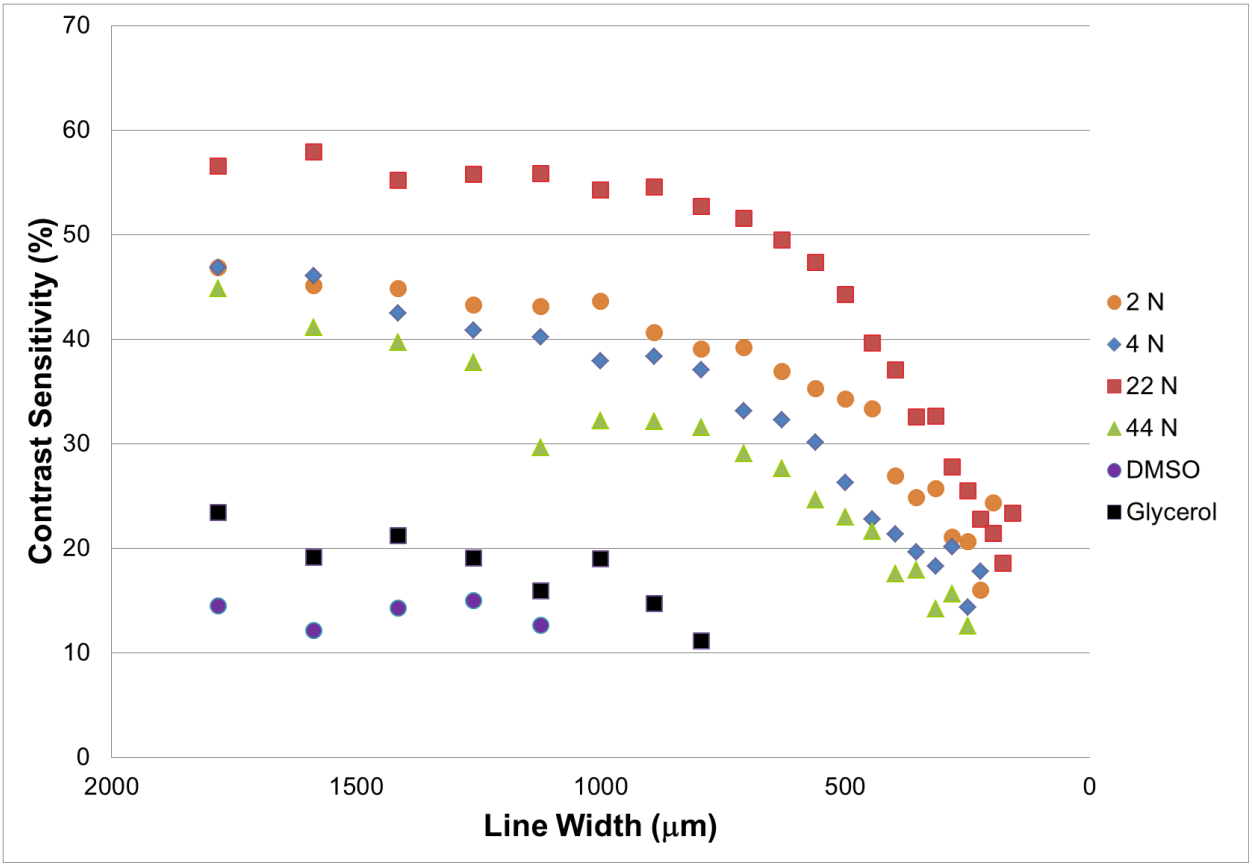

Figure 2-7: Contrast sensitivity as a function of line width for all clearing techniques. Standard error was ~20-35% of the mean contrast sensitivity, therefore there was no statistically significant difference between loading conditions. Error bars omitted for clarity.

2.3.2 Light Transmission Study

Results of simultaneous tissue thickness, load, and optical power transmission through three representative compressed skin specimens are shown in Figure 2-8. As seen in Figure 2-8a, the specimens had initial thicknesses of ~1.80 mm (red), ~1.10 mm (blue), and ~0.85 mm (green). The specimens were compressed at a rate of 0.02 mm/sec (approximate strain rate of ~10^{-2}/sec) until they each reached a final thickness of 0.5 mm. The load applied to each of the specimens (Figure 2-8b) as well as the strain experienced by each specimen was different due to their varying initial tissue thicknesses (i.e., thinner specimens underwent lower strain and required a lower load to reach the final tissue thickness, while thicker samples were strained more and required a higher load to achieve the same final tissue thickness).

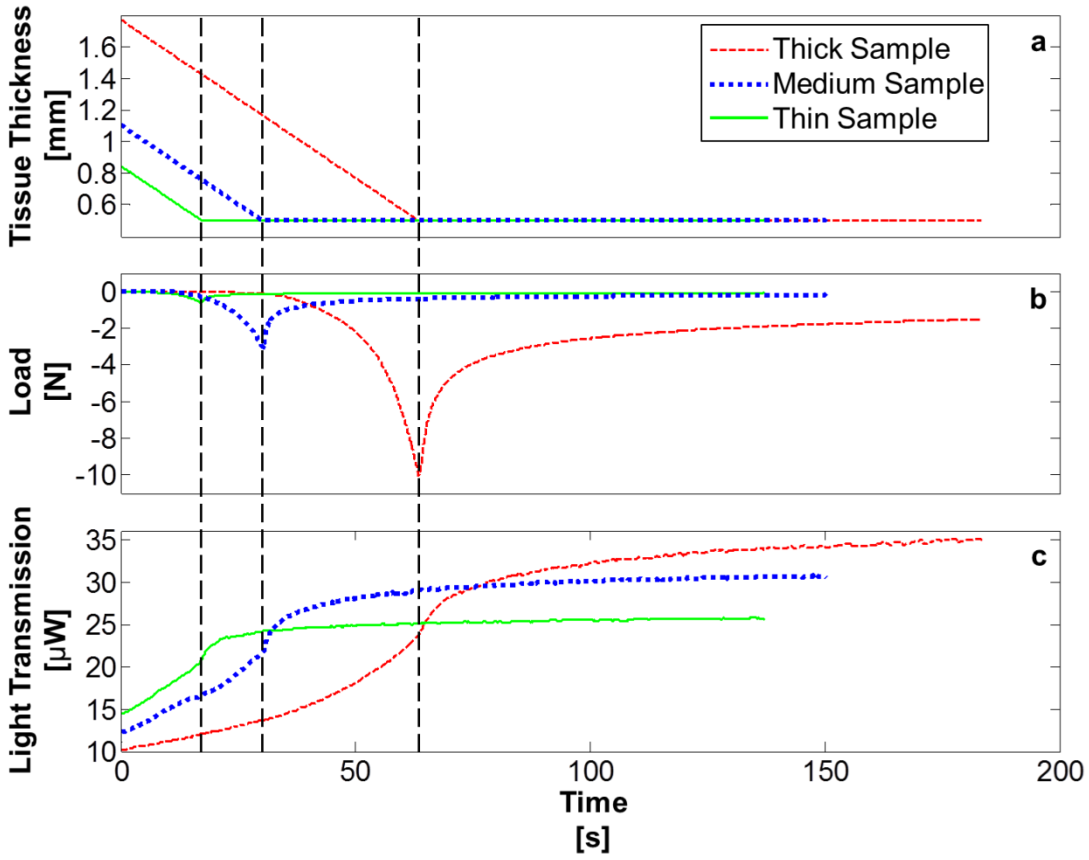

Figure 2-8: Dynamic plots of (a) Tissue thickness, (b) Compressive load, and (c) Light transmission through representative localized compression specimens.

Figure 2-8c shows that a sample with lower initial tissue thickness (green) allowed higher light transmission in the uncompressed state (t = 0). Conversely, a sample with higher initial tissue thickness (red) allowed less light transmission at t = 0. Immediately after each sample was compressed to a final thickness of 0.5 mm (shown by vertical dashed lines), power transmission through all three samples was close to 22 μW. However, after the tissue thickness was held constant at 0.5 mm for two minutes, the power transmitted through the tissue samples continued to increase, but by different amounts depending on initial thickness. Final power transmission for the 0.85 mm, 1.15 mm, and 1.80 mm initial tissue thickness samples was 25 μW, 30 μW, and 35 μW, respectively. The thinnest samples, which initially allowed the highest absolute power transmission, resulted in the lowest absolute power transmission after the constant thickness dwell. The thickest samples, which initially allowed the lowest absolute power transmission, allowed the highest absolute power transmission after the constant thickness dwell.

2.4 Discussion

2.4.1 Mechanical vs. Chemical Tissue Clearing

Resolution of targets through ex vivo porcine skin was assessed to determine the efficacy of localized mechanical compression at different applied loads as a technique to increase image resolution. For comparison to more conventional "chemical clearing techniques", we also performed imaging experiments for tissue specimens immersed in anhydrous glycerol or anhydrous DMSO. We observed significantly higher contrast sensitivity and maximum resolution in all "mechanically cleared" specimens compared to chemically cleared specimens. Figure 2-7 shows that mechanical optical clearing achieved up to ~4 times higher maximum resolution and 2 to 3 times higher contrast sensitivity than immersion in glycerol or DMSO. Standard error was less than ~30% of the mean contrast sensitivity, however there was no statistically significant difference between any of the loads considered. Maximum image resolution was found to correlate inversely with effective tissue strain, as shown in Figure 2-9.

These results indicate that mechanical optical clearing could enhance a myriad of different diagnostic sensing or imaging techniques. Confocal fluorescence microscopy, which is being investigated for the diagnosis of epithelial precancerous lesions, is limited to a maximum imaging depth of close to 500 μm [25, 36-38]. We have shown that our mechanical optical clearing technique allows brightfield imaging through the full epithelial thickness of skin (~2 mm). We believe that mechanical clearing may increase the imaging depth of *in vivo* confocal microscopy, enabling the detection of deeper precancerous lesions thereby resulting in a significant enhancement to real-time *in vivo* diagnostics.

2.4.2 Importance of Tissue Thickness Reduction

In both mechanically compressed and chemically immersed specimens, a reduction in tissue thickness was observed, either in the local compression region in the case of mechanical clearing or over the entire specimen in the case of chemical clearing. Figure 2-9 shows maximum resolvable line width and effective compressive tissue strain for each clearing technique. The specimens used in the 2 N and 22 N cases experienced, on average, a greater compressive strain than the 4 N and 44 N loading cases. This may explain why the 2 N and 22 N compression cases

resulted in higher contrast sensitivity and maximum resolution than the other mechanical loading cases. This data suggests that mechanical clearing may be a function of relative tissue thickness reduction (strain), and not simply the absolute tissue thickness reduction due to the load applied. Figure 2-9 shows the inverse correlation between maximum resolvable line width and effective tissue strain for multiple mechanical loads and chemicals tested.

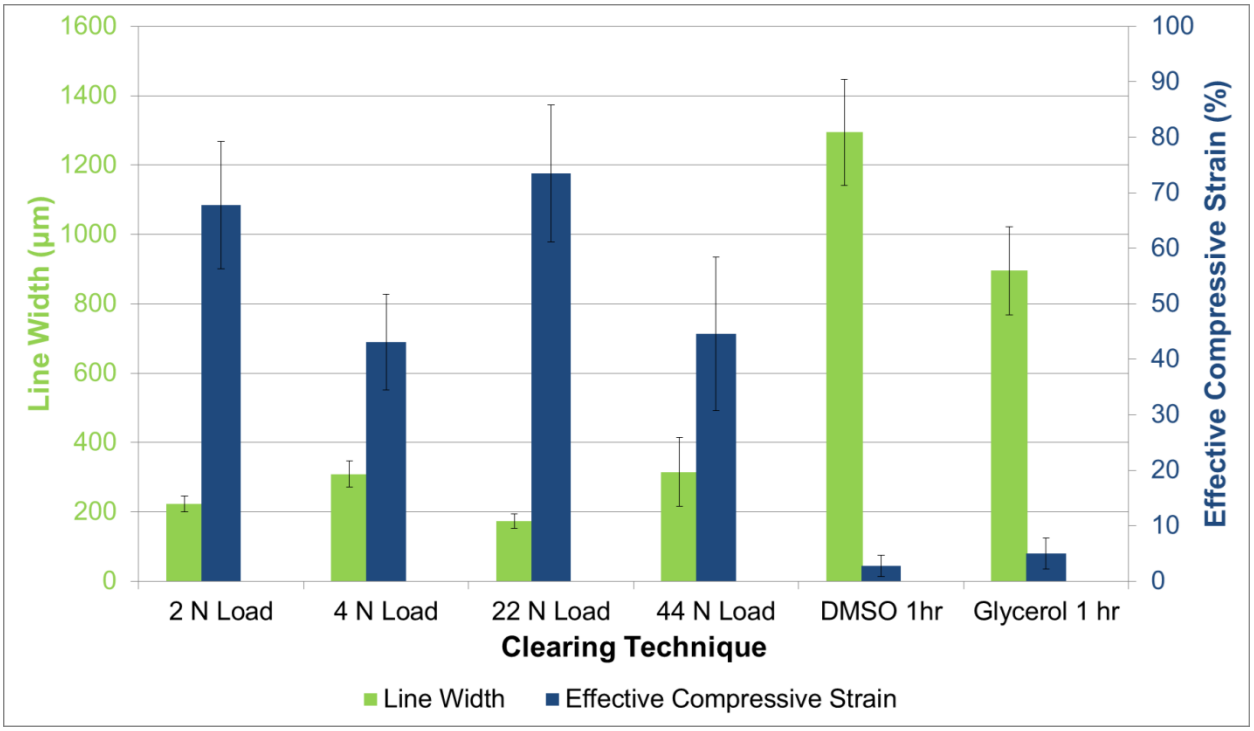

Figure 2-9: Maximum resolvable line width and effective compressive tissue strain for each clearing technique.

Results indicate that mechanical compression achieved a greater increase in resolution and contrast than chemical immersion for the specific methods used in this study. Tissue thickness reduction may be the most important factor influencing this increase in resolution and contrast. Tissue samples experiencing a higher effective compressive tissue strain allowed imaging of smaller target elements and resulted in greater contrast sensitivity than tissue samples experiencing less compressive tissue strain. Chemically cleared specimens had significantly less thickness reduction, but this may be because specimens were only immersed in optical clearing agents for 1 hour.

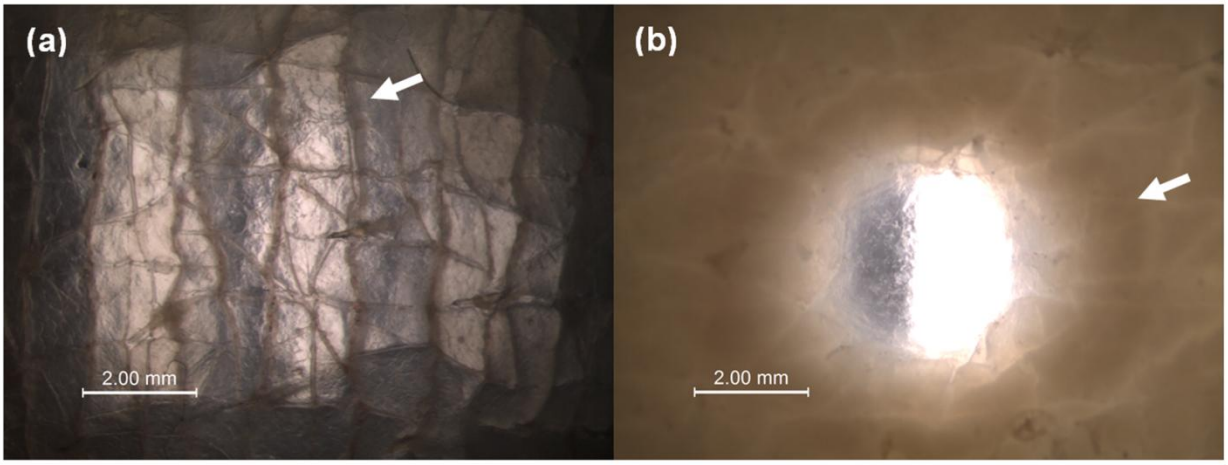

Figure 2-10: Differing morphologies of (a) chemically cleared and (b) mechanically cleared tissue specimens. White arrows indicate areas where structural modification is evident.

2.4.3 Tissue Morphology

We observed that chemically immersed tissue specimens had a different morphology than both mechanically cleared specimens and native tissue. As shown in Figure 2-10a, chemically cleared tissue specimens presented larger ridge-like wrinkle structures not seen in native or mechanically cleared tissue. These features severely impeded visualization of the target bars because they create dark artifacts that make definition of a contrast boundary difficult during image analysis. The presence of these features in chemically immersed specimens prompted the development of the alternate ROI selection technique, described previously, to avoid analyzing regions that would bias the results (such as an apparent high contrast ratio due to the presence of a dark ridge over an element bar, as shown in Figure 2-10a. Analysis using ROI method 1 would not yield any resolvable bars when imaging higher resolution elements through chemically cleared samples. Mechanically compressed specimens were analyzed using both ROI methods 1 and 2, resulting in identical results. We observed that all mechanically compressed tissues were comprised of a central cleared region surrounded by a ring of tissue more turbid (scattering) than the native uncompressed tissue, as shown in Figure 2-10b. This increase in turbidity may be caused by water accumulation. As water is displaced laterally from the compression region under the glass rod, the water content must increase in the area adjacent to the compression region. Mechanically compressed specimens exhibited a smooth surface, which may provide additional advantages for light-based diagnostics.

2.4.4 Mechanisms of Mechanical Optical Clearing

Tissue dehydration and water displacement have been previously identified in chemical clearing studies as potential mechanisms for tissue optical clearing [13, 15, 17, 19, 20, 39]. Based on our understanding of this mechanism, we have investigated a mechanical technique for inducing water displacement and modifying optical properties in tissue. Tissue thinning should contribute greatly to the increase in light transmission through tissue when employing localized mechanical compression because the optical pathlength is shortened. Our previous modeling study [40] has suggested that while tissue compressive strain significantly contributes to the total mechanical optical clearing effect, this contribution is not enough to match experimentally determined light transmission increases during localized mechanical compression. During displacement-controlled loading experiments, we observed that light transmission through the tissue continued to increase even though the tissue thickness was held constant. This suggests that the mechanisms of mechanical optical clearing must include more effects than simple thickness reduction. One candidate for such a mechanism is local tissue dehydration through the lateral expulsion of water out of the compressed region, although more work remains to be done to concretely identify the mechanism of mechanical optical clearing.

Previous studies have investigated effects of mechanical compression on tissue optical properties and light transmission with mixed results [14, 18, 21]. Some researchers have shown increased scattering coefficients due to compressive loading, leading to diminished light transmission through biological tissue [24]. An increase in scattering coefficient reduces the ability to resolve a target through biological tissue. These results disagree with our hypothesis of increased light transmission and higher resolution and contrast sensitivity obtained through mechanical loading. It is important to note, however, that these previous studies delivered a uniform pressure across a large tissue sample (~400 mm^2) sandwiched between glass slides. In this study, however, we applied localized compression over a smaller area (7 or 19 mm^2). This localized loading may enable increased lateral expulsion of water and other light scattering tissue constituents from the compressed region, increasing resolution of a target through the tissue as well as light transmission, which is consistent with our results.

2.5 Conclusion

To the best of our knowledge, we have provided the first demonstration of enhanced target image resolution and contrast through biological tissue using a non-invasive localized mechanical compression technique. We have demonstrated that employing this technique on *ex vivo* porcine skin causes a marked increase in the ability to resolve a target image. With higher tissue strain, resolution and contrast sensitivity of the resolved image is improved. We have also presented evidence supporting the hypothesis that mechanical tissue optical clearing effects are due to both tissue thinning and an additional mechanism, which may be local tissue dehydration through lateral water expulsion.

Optical clearing techniques and devices based on mechanical compression could provide major improvements to optical imaging modalities. Compared to chemical tissue clearing (by delivery to the epithelium surface), mechanical compression could allow visualization of targets that are up to ~4 times smaller with 2 to 3 times higher contrast sensitivity. Localized mechanical compression induces tissue optical clearing in a non-invasive manner without use of exogenous chemicals, but the mechanisms that cause increased resolution and contrast are not fully understood. In the future, we will investigate these mechanisms in more detail. This understanding will enable us to further develop and improve translatable diagnostic or therapeutic devices utilizing this mechanical optical clearing technique.

2.6 Acknowledgements

The authors would like to acknowledge the United States Air Force Office of Scientific Research for a travel grant awarded to present this research at the 30th Annual American Society for Lasers in Medicine and Surgery Conference in Phoenix, Arizona during April 2010. Additionally, we thank the Virginia Tech Initiative to Maximize Student Diversity, funded by NIH Behavioral and Biomedical Sciences and Engineering Research Training Grant R25 GM072767 as well as the Bioengineering/Bioinformatics Summer Institute at Virginia Tech (BBSI), funded by NIH/NSF Award Number 0609225. William C. Vogt is supported by the Institute for Critical Technology and Applied Science (ICTAS) Doctoral Scholars Program at Virginia Tech.

Chapter 3: Effects of Localized Compression on Diffuse Reflectance Spectra of *Ex Vivo* Porcine Skin

Alondra Izquierdo-Román[1], William C. Vogt[1], John L. Robertson V.M.D., Ph.D. [2], Liang Lim[3], Brandon Nichols[3], James W. Tunnell Ph.D[3], Christopher G. Rylander Ph.D[1,4]

[1]School of Biomedical Engineering and Sciences, Virginia Tech, Blacksburg, VA 24060
[2] Department of Biomedical Sciences & Pathobiology, Virginia-Maryland Regional College of Veterinary Medicine, Blacksburg, VA 24061
[3] Department of Biomedical Engineering, The University of Texas at Austin, Austin, TX 78712
[4] Department of Mechanical Engineering, Virginia Tech, Blacksburg, VA 24060

Background and Objectives: Localized mechanical compression has been shown to increase light transmission through turbid tissue. In this study, we investigated the effects of localized compression and indentation geometry on the optical properties of *ex vivo* porcine skin specimens by dynamically monitoring diffuse reflectance spectra and load while controlling tissue thickness.

Study Design/Methods: A custom-built Diffuse Reflectance Spectroscopy (DRS) system was used to monitor the diffuse reflectance spectra from *ex vivo* porcine skin specimens undergoing localized compression. A custom DRS probe was designed which performs both optical sensing and mechanical indentation. Probe tip geometry was varied by bonding 3-6 mm diameter spheres to the DRS probe. A mechanical load frame was used to control probe displacement and resultant specimen thickness change. Diffuse reflectance spectra were recorded during "ramp-and-hold" indentation tests where tissue specimens were displaced to and held at progressively smaller thicknesses. Dynamic thickness, load, and light transmission were simultaneously recorded during the compression protocol. Tissue optical properties were extracted using a previously established look-up table (LUT) approach.

Results: *Ex vivo* compression resulted in a transient increase in light transmission during holds at constant tissue thickness. Reflectance decreased at shorter wavelengths and increased at longer wavelengths with decreasing thickness. The magnitude of change in reflectance correlated with the indenter geometry, with smaller area compression resulting in greater change. Average absorption and reduced scattering coefficients decreased while the tissue was held at 1 mm and 0.5 mm, but increased when the tissue was held at 0.25 mm.

Conclusion: Localized mechanical compression of *ex vivo* porcine skin specimens resulted in thickness-independent, transient changes in light transmission, diffuse reflectance, and optical properties. This suggests there are complementary effects which contribute to changes in optical properties, aside from tissue thinning. With appropriate indentation geometry, localized mechanical compression may be harnessed to controllably modify tissue optical properties and enhance various light-based diagnostic and therapeutic applications.

Key words: spectroscopy; compression; optical clearing; scattering coefficient; inverse model; look-up table;

3.1 Background and Objectives

Light-based diagnostic and therapeutic procedures are severely limited by the penetration depth of light in tissue. The various constituents that make up this heterogeneous structure induce multiple scattering of incident light, reducing the energy delivered to a particular target [18, 19, 24, 25]. A significant amount of research has been devoted to the development of "tissue optical clearing" techniques that aim to overcome the limitations caused by this natural tissue-light interaction. "Tissue optical clearing" refers to the modification of optical properties in biological tissue so as to allow the delivery of near-collimated light deeper into the tissue. Tissue optical clearing could potentially improve numerous optical diagnostic and therapeutic techniques, including optical coherence tomography (OCT), *in situ* confocal microscopy, reflectance spectroscopy, photodynamic therapy (PDT), and other light-based cosmetic procedures [14, 15, 21, 23-26].

Past research has investigated the tissue optical clearing effects of two different methods: chemically-based optical clearing and mechanically-based optical clearing. Chemical optical clearing is achieved by the delivery (topical or injected) of hyperosmotic chemical agents, such as dimethyl sulfoxide (DSMO), glycerol, and glucose [15, 18, 19]. The hypothesized mechanisms of action for chemical clearing include tissue dehydration, refractive index matching, and/or the structural modification or dissociation of collagen fibers [12, 14, 15, 18, 19]. These three mechanisms may work synergistically to modify the optical properties of biological tissue, reduce light scattering, and increase the delivery of near-collimated light deeper into the tissue. Mechanical optical clearing is achieved by locally compressing tissue, and is thought to result from interstitial water and blood displacement leading to local tissue dehydration [15, 21, 23, 40]. As tissue is compressed, water and blood are displaced laterally from regions undergoing high compressive stress. This causes the local ratio of water to proteins and sugar to decrease, resulting in an overall reduction of the refractive index mismatch between constituents and lower scattering and absorption. Although these two tissue optical clearing methods have similar mechanisms of action, mechanical optical clearing techniques seems advantageous due to the preservation of the stratum corneum integrity and fast, localized effects [14, 26].

Although much of the research work has been devoted to the development and assessment of tissue optical clearing procedures, existing spectroscopic techniques have not been employed to systematically evaluate the optical clearing effects induced by the use of these procedures. Quantifying the changes in optical properties using diffuse reflectance spectroscopy would add to our understanding of the effects induced by tissue optical clearing techniques. Diffuse reflectance spectroscopy (DRS) is a well-established, minimally-invasive technique that allows the optical detection of physiological changes in biological tissue [36, 41]. DRS enables the analysis of tissue structure and physiological activity by providing wavelength-dependent measurements of backreflected light. DRS measurements in combination with appropriate computational models or look-up-tables have been used to extract quantitative values of tissue optical properties [42-47]. These properties include absorption and reduced scattering coefficients, which allow estimation of numerous physiological parameters such as blood volume fraction, oxygen saturation, melanin content, and blood vessel diameter [42, 43]. The ability to analyze biological tissue quickly in a minimally invasive and non-destructive manner makes DRS an attractive tool for the rapid diagnosis of tissue disease state *in vivo* and the assessment of treatment response of cancers [48, 49]. This optical technique and tool has been used to obtain diagnostic information *in vivo* from skin, colon, gastrointestinal tract, cervix, and other epithelial tissues [47, 50-55].

Clinical and experimental fiber optic DRS measurements are obtained by illuminating the tissue of interest with a light source through an emitting optical fiber contained in a probe in contact with the tissue. Light remitted from the tissue surface is then collected by an adjacent collecting fiber (multiple fibers may also be used) and analyzed by a spectrometer to generate a diffuse reflectance spectrum. Fiber probe contact with the interrogated tissue is necessary to eliminate unwanted specular reflection [56]. Probe pressure variations due to user variability have been documented by clinicians studying spectral diagnosis techniques [36, 57, 58]. Pressure induced by fiber probe contact may alter the structure and function of tissue in the compressed region, which could likely modify tissue spectral response. This poses a major concern for researchers and clinicians, as pressure effects could distort the true diffuse reflectance signature of the tissue and increase the potential for wrong diagnoses. Thus, scientists are currently investigating probe pressure effects on DRS spectra to understand the potential introduction of error into clinical measurements [36, 37, 42, 53, 56-59].

Various groups have reported the effects of probe pressure on *in vivo* diffuse reflectance spectra. Lim, *et al.*, concluded that errors due to short-term light probe pressure effects (<9 kPa) on human skin were within ±10% for extracted physiological properties and less than ±5% for parameters that were critical for disease diagnosis. Absorption decreased due to the lateral expulsion of blood from the compressed region, though changes in reduced scattering coefficient were site-specific [42]. Chen, *et al.*, studied changes in diffuse reflectance of *in vivo* human skin in the near-infrared region and reported that contact pressure may cause a distortion of the internal tissue structure and alter the distribution of constituents, leading to disturbances in diffuse reflectance spectra measurements [56]. They concluded that diffuse reflectance intensity decreases with increasing contact pressure for their particular probe geometry and wavelength range studied [60]. *In vivo* human skin results presented by Delgado-Atencio, *et al.*, supported Chen's conclusion, but added that reflectance decreases with increasing pressure at longer wavelengths (>600 nm) and increases with increasing pressure at wavelengths less than 600 nm [36]. The probe geometry used in Delgado-Atencio's study consisted of a central source fiber surrounded by a peripheral detector fiber bundle with a source-detector separation of 600 µm. Ti, *et al.*, studied the changes in diffuse reflectance spectra of rat heart and liver tissue *in vivo* and reported a decreasing trend in diffuse reflectance spectra intensity acquired over a period of two minutes for higher probe pressures (~50 mN/mm^2). Lower pressures were not able to replicate this trend. Furthermore, changes in spectral intensity were found to be site specific, with level of vascularization playing a significant role in spectral intensity modification [37]. Various other groups have reported effects due to fiber probe pressure, angle, and duration of contact, with similar results depending on tissue morphology and site tested [53, 58, 59].

The goal of the current study was to investigate the effects of localized mechanical compression and indenter geometry on the optical properties of *ex vivo* porcine skin. Our previous work has shown increases in light transmission, resolution, and contrast sensitivity through *ex vivo* porcine skin as a result of localized mechanical compression [22, 61, 62]. One of these studies highlighted the thickness-independent optical clearing effect of localized compression on *ex vivo* porcine skin specimens [62]. Increased light transmission was found to correlate with tissue strain, with greater strain resulting in greater absolute light transmission increase during localized compression. More importantly, light transmission continued to increase while holding the tissue in compression at constant thickness, indicating that

mechanisms other than tissue thinning affected light transmission increase through the tissue. These experiments, however, did not monitor intrinsic optical property changes during compression. Additionally, the effects of probe geometry on tissue optical property changes during compression have not been investigated. We have seen the effects of indentation geometry *in vivo* (Figure 3-1) after indenting the volar forearm skin of volunteers with two different indenter geometries.

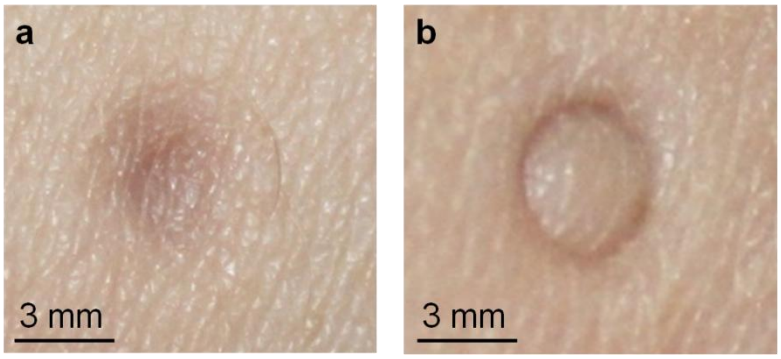

Figure 3-1: In vivo human volar forearm skin indentation. (a) Volar forearm after thirty seconds of compression with a 3 mm diameter hemispherical indenter. (b) Volar forearm after 30 seconds of compression with a 3 mm diameter flat indenter.

Figure 3-1a shows a centrally compressed skin region, appearing darker, following compression with a 3 mm diameter hemispherical indenter. Figure 3-1b shows the stress concentration region resulting from compression with a 3 mm flat tip indenter and the lighter center of this compressed region. The difference in darkness between the centers of both compression regions suggests that the optical properties in these areas are not the same. This may be an effect of stress concentrations in the tissue due to the indenter geometry. Given our observations and past light transmission study results, our current study explored the dynamic effects of different pressures and probe tip geometries on tissue optical properties during localized compression. Diffuse reflectance spectra of *ex vivo* porcine skin specimens were obtained during a displacement-controlled compression protocol using three different probe tip geometries: a flat tip and two hemispherical tips of different diameters. Tissue thickness, load, light transmission, and diffuse reflectance spectra were simultaneously recorded during the compression protocol and tissue optical properties were extracted from the diffuse reflectance spectra using a previously described inverse look-up table model [43, 44]. We hypothesize that localized compression will induce local optical clearing effects in the tissue, resulting in a reduction of the absorption and

reduced scattering coefficients. We anticipate greater changes in optical properties when compressing the tissue with hemispherical indenters, with greater effects occurring with the smaller surface area probe tips.

3.2 Materials and Methods

3.2.1 Skin Specimen Preparation

Ex vivo porcine skin specimens were obtained for experimentation, immediately chilled, and then used within 48 hours of harvesting. The skin specimens were prepared by removing the adipose layer with sharp dissection, using a razor blade. Resulting specimens, consisting of the dermal and epidermal layers of the skin, were approximately 1.01 ± 0.23 mm thick, with a thickness range between 0.72 mm and 1.58 mm. After being trimmed to 2 cm x 2 cm squares, they were stored for no more than 2 days at 4 ºC in a phosphate buffered saline (PBS) moistened container prior to experimentation. Specimens were allowed to equilibrate to room temperature for 30 minutes prior to compression. Initial thickness was determined using the BOSE® ElectroForce® mechanical load frame during experimentation.

3.2.2 DRS System

A custom-built diffuse reflectance spectrometry system (Figure 3-2) was used to collect white light diffuse reflectance spectra from *ex vivo* porcine skin specimens during dynamic compression tests. Broadband light from a tungsten lamp (Ocean Optics LS 1; Dunedin, Florida) was delivered to the tissue via an emitting optical fiber within the custom probe. A collecting fiber adjacent to the emitting fiber collected remitted light and delivered it to a UV-VIS spectrometer for digitization (Ocean Optics USB 2000+ UV-VIS, Dunedin, Florida).

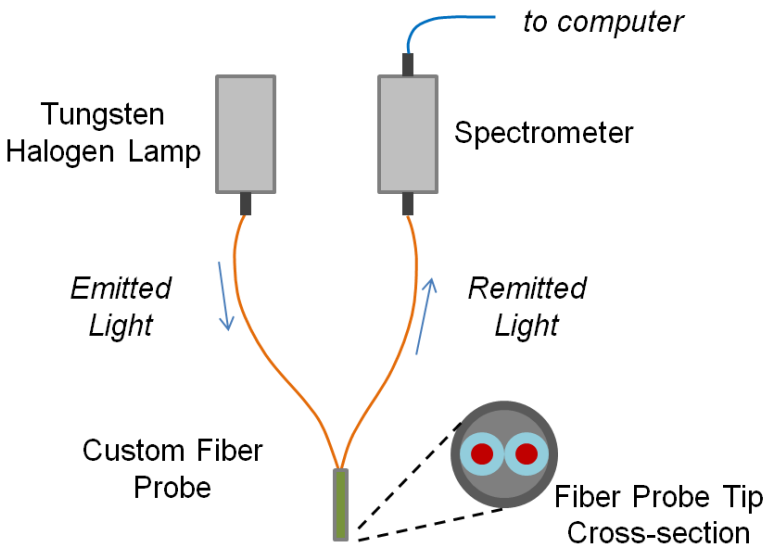

Figure 3-2: DRS system schematic.

3.2.3 DRS Probe

The custom DRS probe built for this study served dual functions: 1) to illuminate the tissue and collect remitted light for reflectance spectra measurements, and 2) to induce mechanical compression on tissue specimens at the distal end of the probe. The fiber probe consisted of two adjacent multimode silica fibers (Thorlabs BFH-22-200, NA = 0.22, 200 µm core diameter, 400 µm cladding diameter, Figure 3-3a placed within a flat-tipped 18 gauge hypodermic needle (0.838 mm inner diameter, 1.27 mm outer diameter)). The fibers were epoxy-bonded within the hypodermic needle and syringe using EPO-MED 030, resulting in a center-to-center source-detection separation of ~400 µm. Previous Monte Carlo modeling studies have shown that this

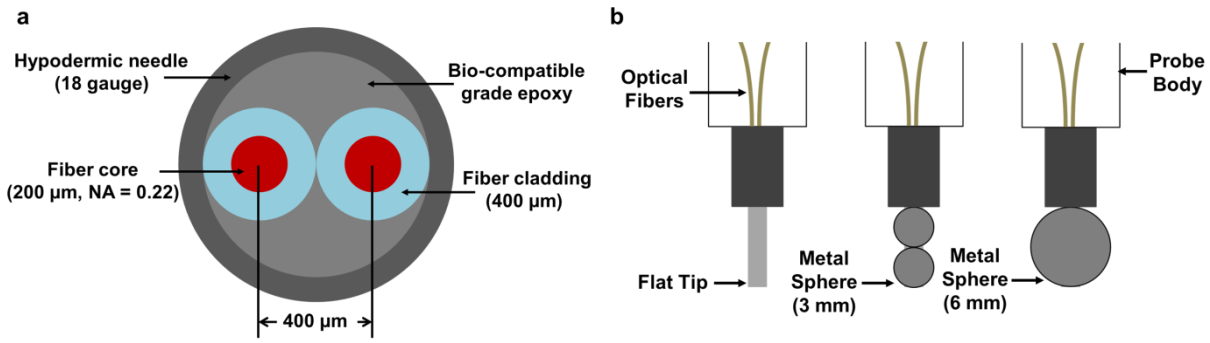

Figure 3-3: (a) Probe tip schematic. (b) Attachments for different probe tip geometries.

source-detector separation results in a depth of interrogation in native tissue between 300 μm and 400 μm [63], which would allow sampling the superficial dermal layer of the tissue. The fibers and hypodermic needle were polished flat at the tip and connectorized with SMA connectors at the proximal end.

The distal end of the fiber probe had a flat, circular surface area of 1.27 mm^2. With simple modification, two additional tip indentation geometries were achieved: a 3 mm hemispherical indentation geometry and a 6 mm hemispherical indentation geometry. These were obtained by gluing a metal sphere (1.3 mm diameter bore through hole) to the hypodermic needle tip (Figure 3-3b). When fit with the 3 mm and 6 mm metal beads, the probe tip maximum cross-sectional area was 7.07 mm^2 and 28.27 mm^2, respectively. The 1.27 mm^2 flat tip area was small relative to the area resulting from the addition of the metal spheres to the tip, making the overall effect on the tissue a hemispherical indentation rather than a flat indentation when the spheres were affixed to the tip.

3.2.4 BOSE-DRS System Integration

The custom DRS probe was designed to interface with a BOSE® ElectroForce® 3100 mechanical load frame. This load frame has a displacement resolution of 1.5 microns over a 5 mm stroke and a force resolution of 6 mN with a 22 N capacity load cell, which provides satisfactory displacement, load resolution, and range for this study. The BOSE-DRS integrated system, shown in Figure 3-4 was used to indent *ex vivo* porcine skin specimens. Displacement-controlled localized compression (resulting in pressures between 0.015 to 10 MPa) was applied to ~1 mm thick porcine skin specimens. During compression, instantaneous diffuse reflectance spectra of the epidermal surface of the specimen were recorded using the DRS probe and system. The custom DRS reflectance probe was housed within a polycarbonate housing connected to the displacement cell of the ElectroForce®. Light was delivered from the tungsten-halogen light source to the specimens while the polycarbonate housing and probe tip moved with the actuated displacement cell downwards, compressing the tissue. Only the probe tip made contact with the skin.

Porcine skin specimens were placed beneath the probe tip on a glass slide which was rigidly fastened above a load cell via an aluminum adapter. A 12.5 mm diameter hole in the aluminum adapter beneath the glass sheet allowed light to be transmitted through the tissue to a large-area photodetector (1 cm x 1 cm), which generated an electrical signal proportional to the light

transmitted through the skin specimens (Newport Detector #818-ST and Optical Power Meter #1931-C). During compression, instantaneous tissue thickness, load, light transmission, and diffuse reflectance spectra were recorded.

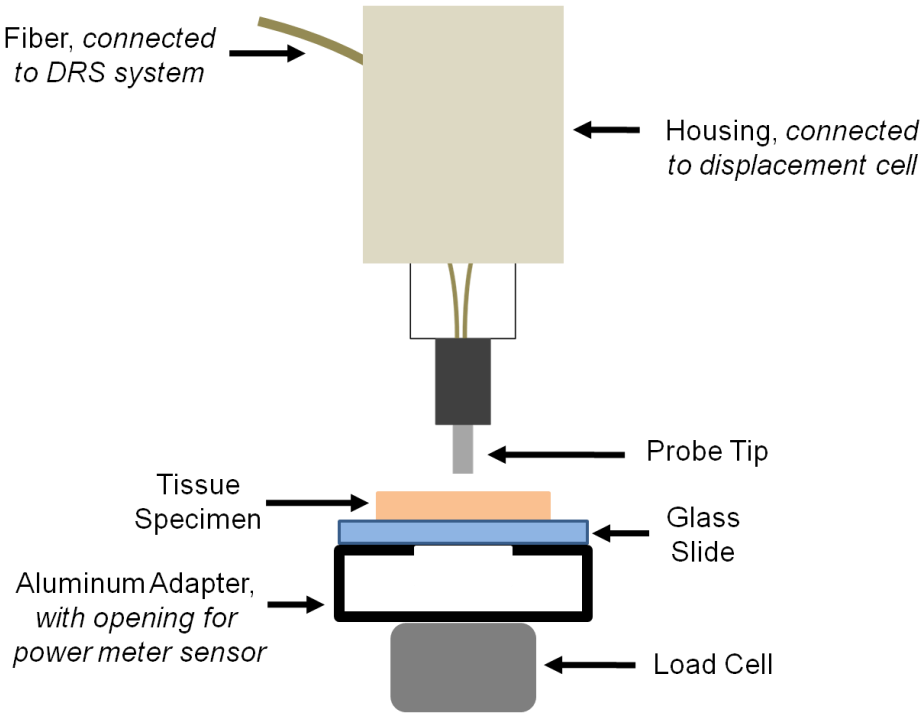

Figure 3-4: Compression experimental components. Diffuse reflectance spectra of ex vivo porcine skin, as well as the force and dynamic tissue thickness, were recorded simultaneously.

3.2.5 Mechanical Compression-Diffuse Reflectance Acquisition Procedure

A compression protocol was developed to study the change in diffuse reflectance spectra (and optical properties) during tissue compression as a function of probe tip shape and diameter (both affecting local stress in the tissue). The protocol consisted of stepped displacement-controlled compression to a maximum of three decreasing thickness levels (depending on specimen initial thickness) with a dwell at each thickness to evaluate thickness-independent as well as transient effects of compression on optical properties. Collection of diffuse reflectance spectra during the loading routine was continuous. This compression protocol was implemented for 33 trials: ten replicates for the 3 mm and 6 mm tip condition each and thirteen replicates for the flat tip condition. The compression protocol consisted of seven separate commands:

1) Ramp displacement to compress the skin specimen to 1.00 mm thick at a displacement rate of 0.02 mm/sec (strain rate of ~10^{-2} /sec);

2) Dwell at 1.00 mm thickness for 180 seconds;
3) Ramp displacement to compress the skin specimen to 0.50 mm thick at a displacement rate of 0.02 mm/sec (strain rate of ~10^{-2} /sec);
4) Dwell at 0.50 mm for 180 seconds;
5) Ramp displacement to compress the skin specimen to 0.25 mm thick at thick at a displacement rate of 0.02 mm/sec (strain rate of ~10^{-2} /sec);
6) Dwell at 0.25 mm for 180 seconds;
7) Unload tissue.

Both initial and dynamic tissue thickness were important parameters in this study. Before each trial, the position of the glass slide was determined by displacing the fiber probe tip downwards until it made contact with the glass slide, and this position, x_g, was recorded. Contact was defined as the position at which the load magnitude exceeded 0.01 N. After the probe tip was returned to its original position, a tissue specimen was placed on the glass slide and the compression protocol was executed. The contact position of the top surface of the specimen, x_c, was calculated in post-processing following the same load threshold definition. Tissue thickness, $T(t)$, was then calculated as

$$T(t) = \left(x_c - x_g\right) - x(t) \tag{3.1}$$

where $x(t)$ is the measured displacement signal at time t. We also define a compressive tissue strain, e, which is the relative deformation of the compression tissue specimen region as

$$e = \frac{|T - T_0|}{T_0} \tag{3.2}$$

where T_0 is the initial tissue thickness and $T(t)$ is the compressed tissue thickness. Displacement, load, light transmission, and diffuse reflectance spectra were recorded for the entirety of the compression protocol at a rate of 10 Hz. Applied force, displacement, and light transmission

were recorded instantaneously during skin compression using WinTest®, the integrated BOSE® control data acquisition software (BOSE; Eden Prairie, Minnesota). Spectral data were acquired using an integration time of 100 ms. Dynamic reflectance spectra were recorded using SpectraSuite® Spectroscopy Platform, the data acquisition software for the Ocean Optics USB2000+ Spectrometer.

3.2.6 DRS Data Analysis

Specimen optical properties were obtained by fitting diffuse reflectance spectra to a lookup table-based (LUT) inverse model, discussed in detail elsewhere [43, 44]. Data calibration is crucial in the LUT inverse model fitting procedure, as described by Rajaram, *et al.* Briefly, differences in daily measurements due to source intensity and system response were accounted for by regular calibration measurement of a standard solution of 1 μm diameter polystyrene microspheres (0.12%; Polysciences, Warrington, Pennsylvania) in water ($R_{beads}(\lambda)$).Performing this calibration ensured that the measured changes in diffuse reflectance were due only to changes in tissue optical properties and tissue morphology. Diffuse reflectance was calculated by using the equation

$$R_{diffuse}(\lambda) = \frac{I_{sample}(\lambda) - I_{background}(\lambda)}{[I_{standard}(\lambda) - I_{background}(\lambda)]} \times 100 \tag{3.3}$$

where $I_{sample}(\lambda)$ is the white light intensity measured from the *ex vivo* porcine skin specimen, $I_{background}(\lambda)$ is a background spectrum measurement recorded with the light sources turned off, and $I_{standard}(\lambda)$ is recorded from a calibrated reflectance standard (Spectralon SRS-99-020, Labsphere, Inc.; North Sutton, New Hampshire). The background spectrum subtraction eliminates the effects of CCD dark current and ambient light. Wavelength-dependent system response is eliminated by dividing the background corrected intensity measurement by the calibrated reflectance standard measurement. The diffuse reflectance spectra for each measurement was then calculated as

$$R_{calibrated}(\lambda) = R_{diffuse}(\lambda) \times \frac{R_{beads\ (LUT)}(\lambda)}{R_{beads}(\lambda)} \quad (3.4)$$

where $R_{beads\ (LUT)}(\lambda)$ was recorded from a solution of polystyrene beads on the same day of the creation of the LUT. Following this procedure, all reflectance measurements were calibrated to the LUT model for extraction of optical properties.

3.3 Results

3.3.1 Light Transmission Results

As described earlier, the compression protocol consisted of compressing *ex vivo* porcine skin specimens to a specific thickness and holding the thickness constant for three minutes while recording the parameters of interest. Three thickness levels were selected for the compression protocol: 1.00 mm, 0.5 mm, and 0.25 mm. Due to differences in initial tissue thickness (some specimens were thinner than 1.00 mm initially), not all trials could satisfy the compression condition to 1.00 mm thickness because required load exceeded system capability. For this reason, specimens of greater initial thickness could not always be compressed to the high load/strain condition of the 0.25 mm final thickness. After completing the compression protocol for the three tip geometry conditions, the data were further examined for any obvious outliers, caused by either acquisition error or poor contact of the fiber optic probe. Twenty-eight trials were chosen for subsequent analysis. Table 3-1 summarizes the total specimen test group size (N) that met each specific thickness condition.

Condition	*3 mm Hemi Tip*	*6 mm Hemi Tip*	*Flat Tip*
Contact	N = 8	N = 9	N = 11
1 mm	N = 5	N = 6	N = 4
0.5 mm	N = 7	N = 9	N = 11
0.25 mm	N = 4	N = 4	N = 8

Table 3-1: Thickness conditions met by probe tip group. “N” denotes total specimen test group size.

Simultaneous tissue thickness, load, and percent light transmission increase through a representative skin specimen compressed with the flat probe tip are shown in Figure 3-5a-c. Three individual dwell periods at constant thickness can be identified in Figure 3-5b, where tissue thickness is held constant at 1.00 mm, 0.5 mm, and 0.25 mm for a period of three minutes each. Figure 3-5c shows the typical non-linear response occurring in light transmission during these dwell periods. Light transmission continues to increase during the hold at constant thickness at the higher strain conditions, *i.e.* when the specimen is held at 0.5 mm and 0.25 mm. Moreover, at higher strain there is more rapid light transmission increase throughout the dwell period. Light transmission while the tissue thickness was held constant at 0.5 mm and 0.25 mm did not plateau during the dwell period. It is interesting to note a brief decrease in light transmission occurring during the compressive ramp to reach the 0.25 mm thickness condition. This dip in light transmission was typical of all trials during the compression ramp to reach higher strain conditions. The plots shown in Figure 3-5 represent the overall trend seen in all compression trials for the three tip conditions. Naturally, the maximum pressure delivered by each tip varied with indenter geometry (Table 3-1). The average relative percent increase in light transmission during each dwell condition (before and after dwell at constant thickness) for different probe tip geometries is shown in Figure 3-6. We define a relative percent increase in light transmission as

$$Relative\ Percent\ Increase = \frac{\left(I_{after\ dwell} - I_{before\ dwell}\right)}{I_{before\ dwell}} * 100 \tag{3.5}$$

where $I_{before\ dwell}$ is the amount of light transmitted through the specimen when tissue thickness initially reached the specific thickness condition (1.00 mm, 0.5 mm, or 0.25 mm) and $I_{after\ dwell}$ is the amount of light transmitted after the three minute hold at constant thickness. During the dwell at 1.00 mm, 0.5 mm, and 0.25 mm, light transmission increased approximately 4%, 31%, and 32%, respectively, for the flat probe tip. During the dwell at 1.00 mm, 0.5 mm, and 0.25 mm, light transmission increased approximately 12%, 30%, and 32%, respectively, for the 3 mm hemispherical probe tip. Finally, during the dwell at 1.00 mm, 0.5 mm, and 0.25 mm, light transmission increased approximately 17%, 37%, and 30%, respectively, for the 6 mm hemispherical probe tip.

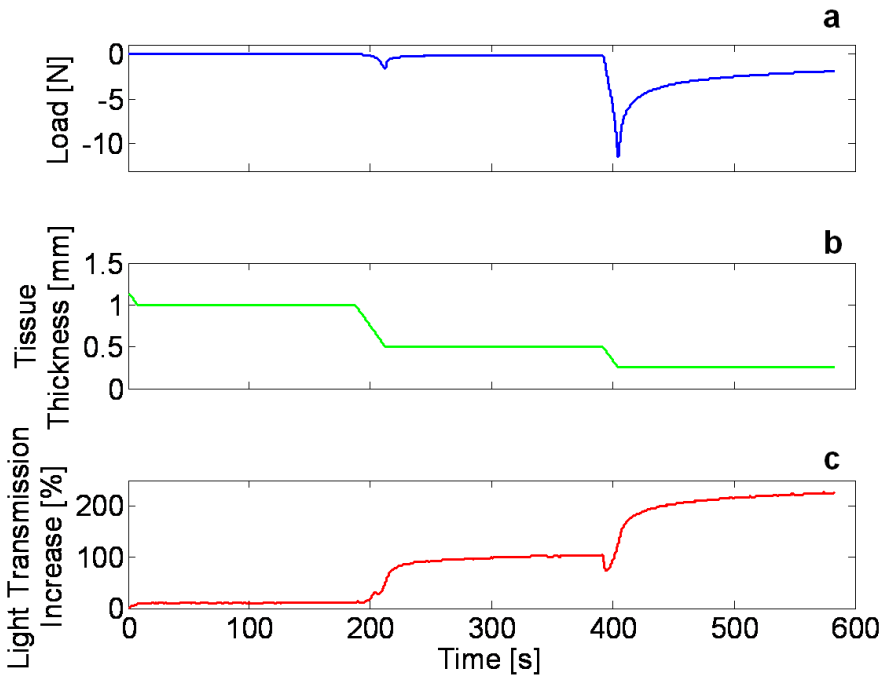

Figure 3-5: Example of the dynamic a) load, b) tissue thickness, and c) percent light transmission increase through a representative tissue specimen. Flat tip geometry.

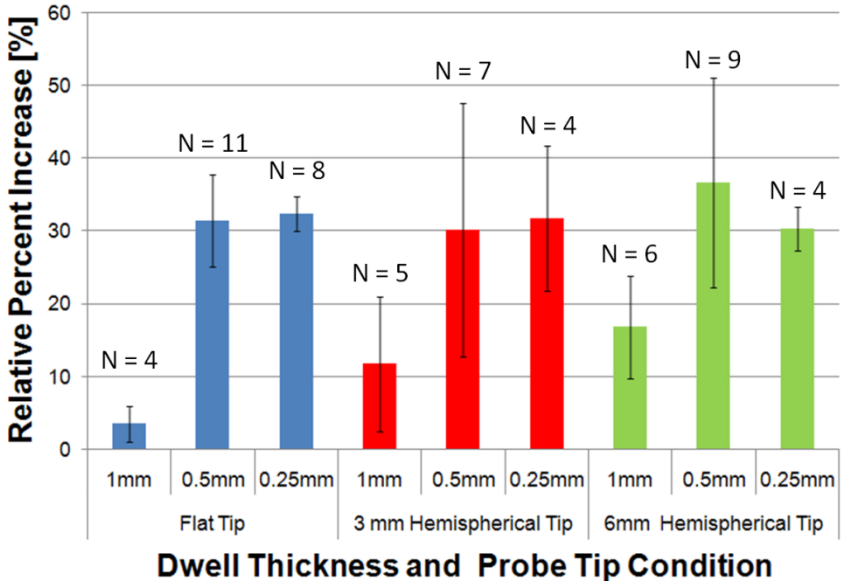

Figure 3-6: Average relative increase in light transmission during each dwell condition for different probe tip geometries.

3.3.2 Reflectance Spectra Results

The average reflectance for specimens compressed with the 3 mm hemispherical indenter, the 6 mm hemispherical indenter, and the flat indenter are seen in Figure 3-7, Figure 3-8, and Figure 3-9, respectively. The plots show the mean reflectance spectra at each compression condition for the different probe tip indenter geometries. These successive plots show the effects of compression on tissue diffuse reflectance during two important stages: (1) immediately after being compressed to a specific thickness (solid blue line) and (2) after the 3 minute dwell period during which tissue thickness was held constant (red dotted line).

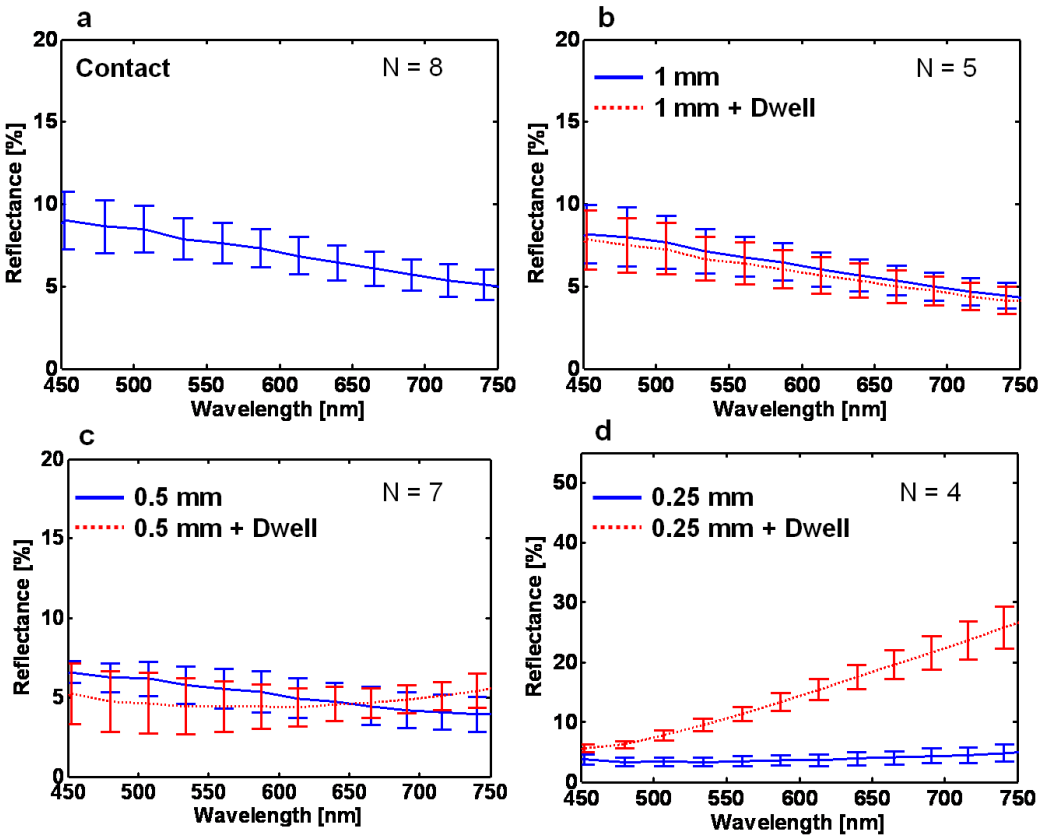

Figure 3-7: Average reflectance spectra for 3 mm hemispherical tip. (a) Reflectance during probe tip contact with skin. (b) Reflectance before and after dwell at 1 mm tissue thickness. (c) Reflectance before and after dwell at 0.5 mm tissue thickness. (d) Reflectance before and after dwell at 0.25 mm tissue thickness.

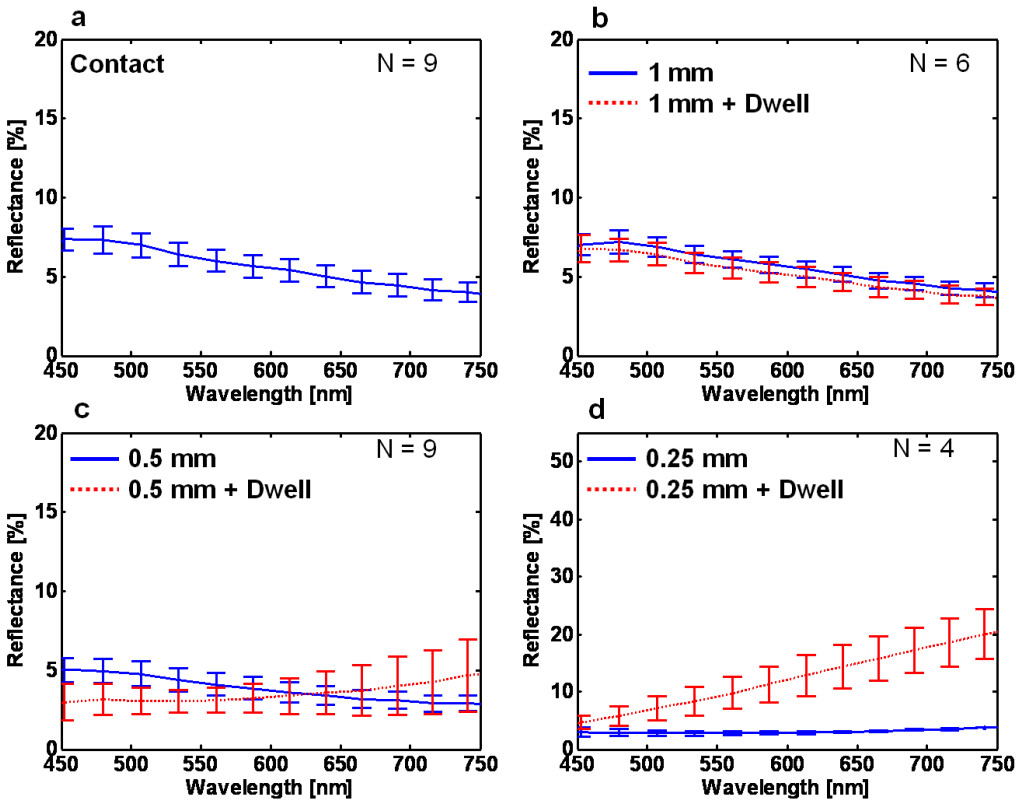

Figure 3-8: Average reflectance spectra for 6 mm hemispherical tip. (a) Reflectance during probe tip contact with skin. (b) Reflectance before and after dwell at 1 mm tissue thickness. (c) Reflectance before and after dwell at 0.5 mm tissue thickness. (d) Reflectance before and after dwell at 0.25 mm tissue thickness.

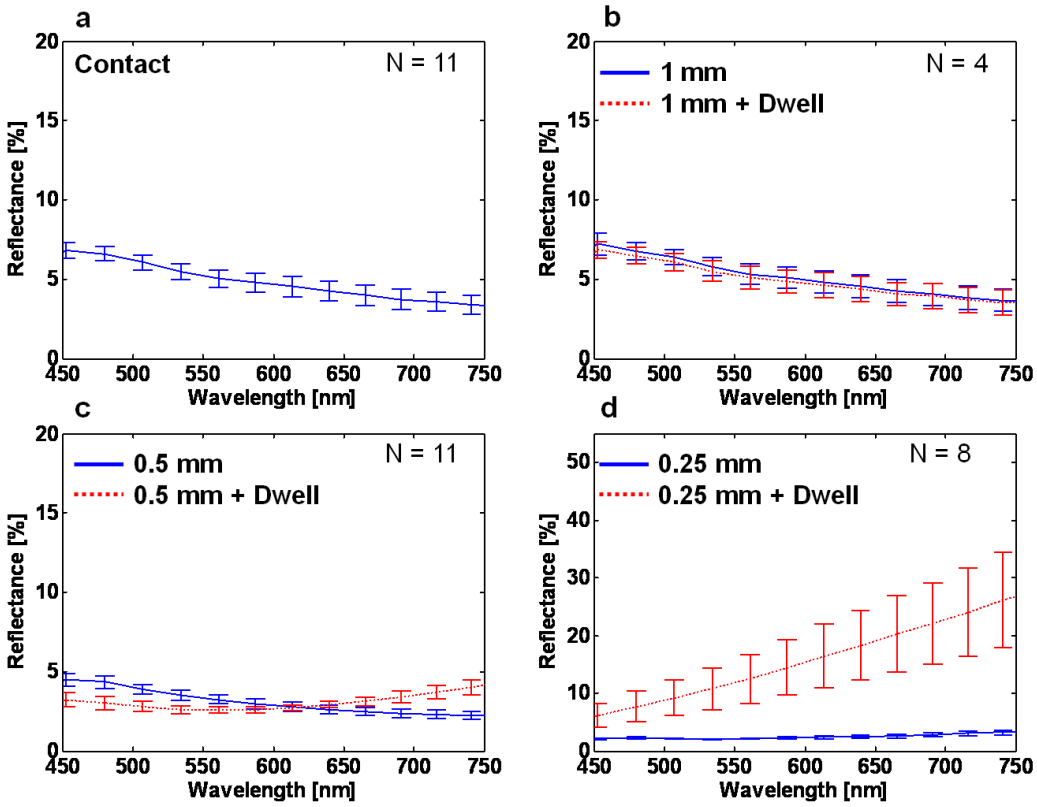

Figure 3-9: Average reflectance spectra for flat tip. (a) Reflectance during probe tip contact with skin. (b) Reflectance before and after dwell at 1 mm tissue thickness. (c) Reflectance before and after dwell at 0.5 mm tissue thickness. (d) Reflectance before and after dwell at 0.25 mm tissue thickness.

Figure 3-7a-d shows the dynamic change in reflectance during the compression protocol with the 3 mm hemispherical tip. When the probe tip was in contact with the tissue, reflectance in the shorter wavelengths was ~9% compared to less than 6% in the longer wavelengths (Figure 3-7a). This was also the case for the 1.00 mm condition before and after the 3 minute dwell at constant thickness (Figure 3-7b). Due to the average initial thickness of the specimens (~1 mm), this first thickness condition resulted in very low strain (14 ±0.09%), which would account for the almost negligible decrease in reflectance after the dwell (Figure 3-7b, dotted red curve). Compression during the ramp to reach the 0.5 mm thickness condition (Figure 3-7c, solid blue curve) resulted in a slight decrease in reflectance to about 6% at shorter wavelengths with an associated average strain of 47 ± 0.12%. During the dwell at 0.5 mm, reflectance at the shorter wavelengths continued to decrease, reaching 5%, while reflectance at the longer wavelengths continued to increase, reaching close to 6% (Figure 3-7c, dotted red curve). The same trend was seen immediately after compressing the tissue to 0.25mm (Figure 3-7d, solid blue curve), although

after the dwell at this thickness condition (Figure 3-7d, dotted red curve), the reflectance at longer wavelengths increased drastically to close to 25%. Average tissue strain at 0.25 mm tissue thickness was 71 ±0.05%. The same overall trends were seen in the diffuse reflectance spectra of specimens that were compressed with the 6 mm hemispherical indenter (Figure 3-8a-d). This tip geometry, however, resulted in a lower average reflectance after the dwell at the final thickness condition of 0.25 mm. For this probe tip, reflectance in the longer wavelengths was close to 20% (Figure 3-8d). Finally, the flat tip geometry also yielded very similar results (Figure 3-9a-d), with higher reflectance occurring after the dwell at the 0.25 mm condition (Figure 3-9d) than with the 3 mm and 6 mm hemispherical indenters.

3.3.3 Extraction of Optical Properties

The average absorption and reduced scattering coefficients (at 630 nm) for specimens compressed with the three different indenter geometries are seen in Figure 3-10 and Figure 3-11, respectively. Absorption in all specimens was very low, and a decreasing trend in μ_a was observed with decreasing tissue thickness (Figure 3-10a-c). Additionally, μ_a decreased transiently while the tissue was held at a fixed position during the three minute dwell periods. The last data point in all trials exhibited a peculiar trend. At this strain condition, three minutes after the tissue had been held at a fixed 0.25 mm of thickness, the absorption coefficient had increased considerably for all probe tip geometries. Without taking into account this last datum, μ_a decreased 89% for the flat tip, 48% for the 3 mm hemispherical tip, and 89% for the 6 mm hemispherical tip between the contact condition (tissue's initial thickness) and the 0.25 mm condition. Transient changes in μ_a, those changes evident while the tissue specimens were held at a fixed thickness, were also evident and are summarized in Table 3-2. Scattering in all specimens was relatively low, and kept decreasing with decreasing tissue thickness, seen in Figure 3-11. A transient decrease in μ_s' also occurred while the tissue thickness was held fixed. Again, the last datum in all trials exhibited a peculiar trend, similar to what was seen for μ_a. At this strain condition, three minutes after the tissue had been held at a thickness of 0.25 mm, the absorption coefficient had increased drastically for all probe tip geometries. Without taking into account this last datum, μ_s' decreased 40% for the flat tip, 37% for the 3 mm hemispherical tip, and 37% for the 6 mm hemispherical tip between the contact condition (at initial tissue thickness) and the 0.25 mm condition. Transient changes in μ_s', occurring during the dwell at constant thickness, are summarized in Table 3-2.

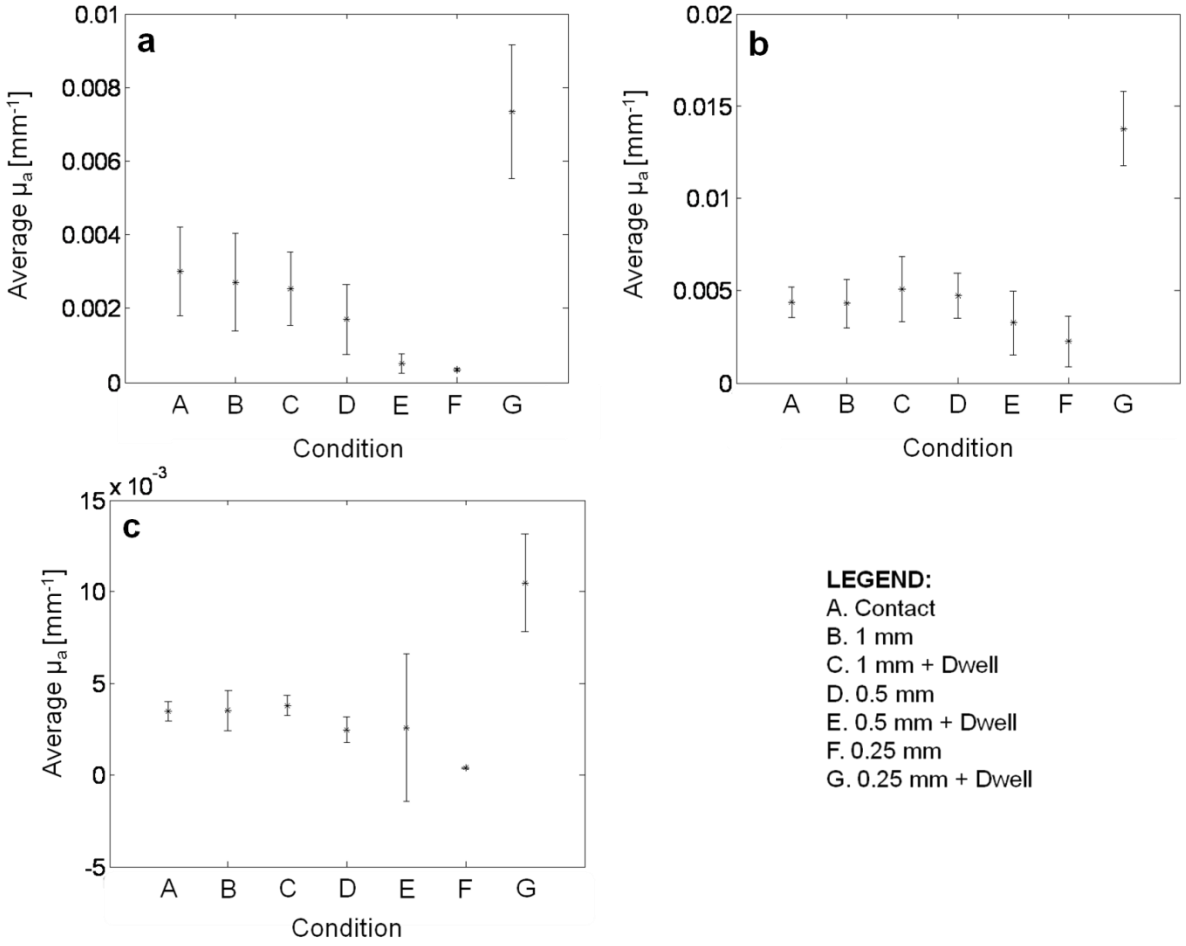

Figure 3-10: Average absorption coefficient at different tissue specimen thickness conditions. (a) Flat tip indenter. (b) 3 mm hemispherical indenter. (c) 6 mm hemispherical indenter.

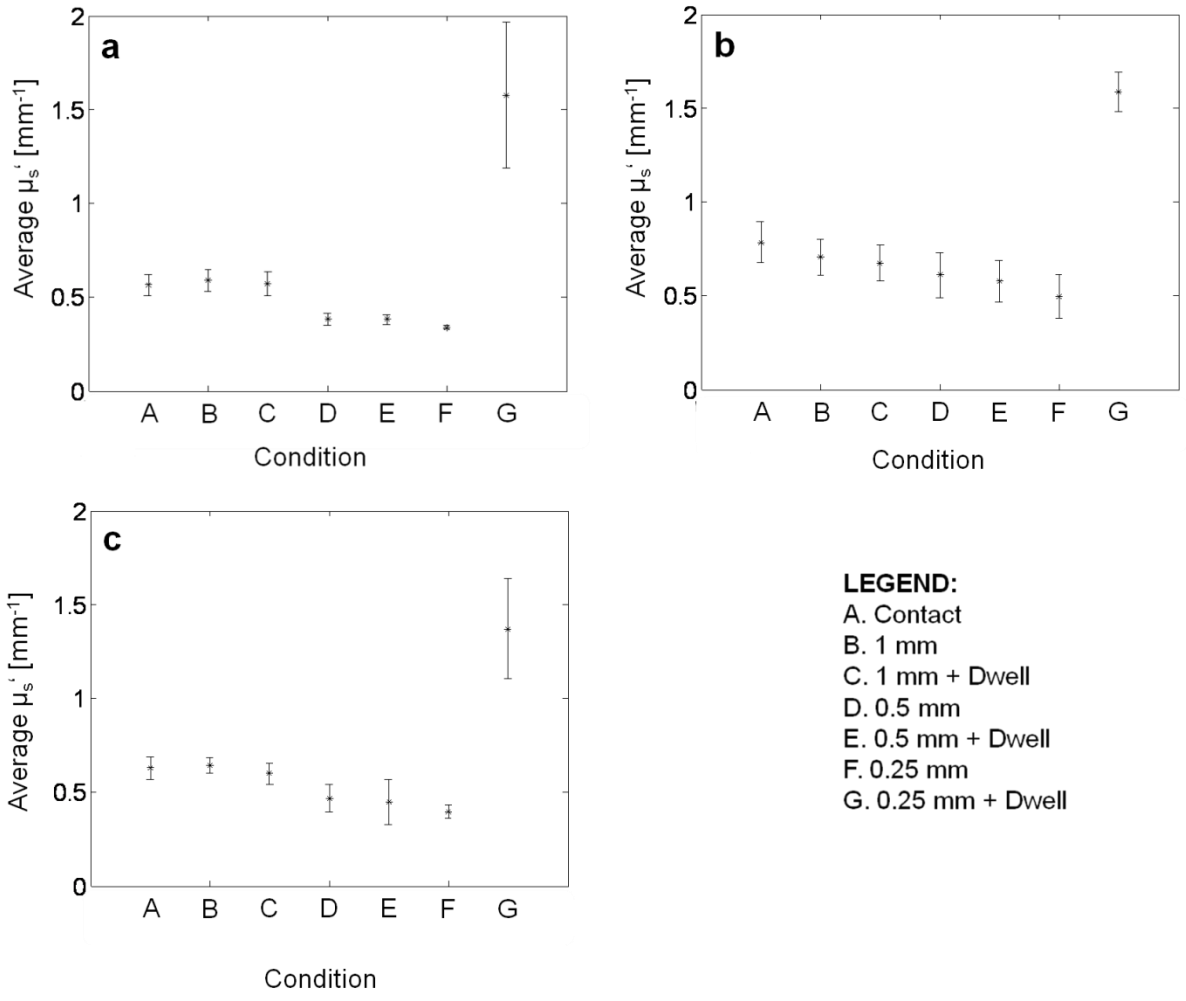

Figure 3-11: Average reduced scattering coefficient at different tissue specimen thickness conditions. (a) Flat tip indenter. (b) 3 mm hemispherical indenter. (c) 6 mm hemispherical indenter.

	Flat Tip		3 mm Hemi. Tip		6 mm Hemi. Tip	
Condition	*Relative Change in* μ_a *[%]*	*Relative Change in* μ_s' *[%]*	*Relative Change in* μ_a *[%]*	*Relative Change in* μ_s' *[%]*	*Relative Change in* μ_a *[%]*	*Relative Change in* μ_s' *[%]*
Contact *to* 1 mm	-11	5	-1	-10	1	2
1 mm *to* 1 mm + Dwell	-6	-3	18	-4	8	-7
1 mm + Dwell *to* 0.5 mm	-33	-33	-6	-9	-34	-22
0.5 mm *to* 0.5 mm + Dwell	-70	0.1	-32	-5	4	-4
0.5 mm + Dwell *to* 0.25 mm	-33	-11	-31	-14	-84	-11
0.25 mm *to* 0.25 mm + Dwell	2028	366	513	220	2578	246

Table 3-2: Average relative change in optical properties between tissue thickness conditions.

3.4 Discussion

In this study, we investigated the effects induced by localized mechanical compression on the optical properties of *ex vivo* porcine skin. We compressed and held tissue specimens at three different thickness conditions, resulting in various levels of compressive strain. Three different probe tip shapes/diameters were tested to induce different applied pressures and local stress states in the skin specimens. During the compression procedure, we simultaneously monitored light transmission, load, dynamic tissue thickness, and diffuse reflectance spectra. We utilized a novel, robust procedure to elucidate the optical clearing effects of localized mechanical compression. Time-dependent measurement of the diffuse reflectance spectra of *ex vivo* porcine skin specimens during the application of localized compression provides insight into the correlation between tissue compression and corresponding changes in optical properties.

Previous work by our group has demonstrated that mechanical optical clearing is a transient, strain-dependent response [62]. Our current study utilized displacement-controlled compression

instead of load-controlled compression as has been previously studied by other groups. With load-controlled compression, changes in optical properties are not easily decoupled from dynamic changes in tissue thickness and constituent geometry. Thus, we aimed to replicate the displacement-controlled compression procedure to reveal thickness independent optical property changes due to transient effects of localized mechanical compression. While our results indicate that there is a change in optical properties during the loading phase of our procedure (due in part to thickness change), transient changes during the constant thickness portion of the procedure were also evident, supporting our hypothesis that changes in tissue optical properties are due to more than just a change in tissue thickness.

Diffuse reflectance decreased with decreasing tissue thickness and associated increase in pressure in the shorter wavelengths and increased at longer wavelengths. The absorption of light by water is higher at the longer wavelengths we studied (~700 nm). Local removal of water induced by compression would cause a reduction in light absorption by water, possibly resulting in an increase in reflectance. This was evident in our results when the tissue was compressed to 0.5 mm, which may have been a result of the efflux of water from the compressed tissue region.

Pressures in our study were significantly higher than those used in studies by other researchers. As pressure is directly related to the surface area of the indenter with which we are compressing, our compression procedure resulted in pressures between 0.015MPa and 10 MPa, depending on the probe tip geometry used. Table 3 summarizes the maximum pressures applied by the different probe tips to the skin specimens for each tissue thickness condition.

		Flat Tip			***3 mm Hemispherical Tip***			***6mm Hemispherical Tip***	
Thickness Condition	1 mm	0.5 mm	0.25 mm	1 mm	0.5 mm	0.25 mm	1 mm	0.5 mm	0.25 mm
Max Pressure [MPa]	0.018	1.11	9.78	0.038	0.788	1.621	0.015	0.388	0.444

Table 3-3: Maximum pressures induced by different probe tip geometries at tissue thickness conditions.

The smaller probe tip diameter of the flat tip resulted in higher pressures when compared to the larger tip diameters of the 3 mm and 6 mm hemispherical indenters. The high pressure was induced rapidly and decreased quickly as the tissue relaxed after the initial ramp to the particular thickness step, seen in Figure 3-5b.

Although changes in the associated optical properties appeared greater with the smallest tip diameter, the flat tip (1.27 mm Ø), followed by the 6 mm hemispherical tip, and finally the 3 mm hemispherical tip, these changes were not statistically significant. The initial transient increase in μ_a that occurred during the dwell at 1 mm using the 3 mm and 6 mm hemispherical indenter, but not seen when using the smaller diameter flat indenter, may be due geometric differences causing a pooling of cellular constituents under the larger area of compression induced with the hemispherical tips. When comparing the two hemispherical indenters, although the absolute change in optical properties was greatest for the 6 mm indenter, the 3 mm indenter compression resulted in a more monotonic reduction of both μ_a and μ_s'. Given that our experiments were performed using *ex vivo* tissue, initial μ_a and μ_s' values at the contact condition for all specimens were relatively low, 0.004 ±0.001 mm^{-1} and 0.649 ±0.12 mm^{-1}, respectively.

Most probe pressure effect studies to date have focused on load-controlled compression of tissue, inducing a constant pressure while recording static and transient diffuse reflectance response [36, 37, 42, 53, 58, 59]. The effects of pressures between ~0.01 MPa to ~0.20 MPa have been investigated by numerous research groups, with varying results depending on the tissue interrogated, the amount of time the tissue was compressed, and the specific geometries and source detector separation of the probes used. Delgado-Atencio, *et al.*, reported decreasing reflectance on *in vivo* human skin with increasing pressure for wavelengths above 600 nm, having induced a maximum pressure of 0.1 MPa over five seconds [36]. Our results indicated decreasing reflectance below 600 nm and increasing reflectance above 600 nm with decreasing tissue thickness. Nonetheless, the probe used in the Delgado-Atencio study had a source-detector separation of 600 µm, which would result in the interrogation of deeper tissue when compared to the sampling depths of our current probe design. Also, the probe incorporated a cylindrical accessory at the tip that had a 170 micron thick glass window to protect the optical fiber tips from deterioration. This attachment made the surface area of the probe tip ~53 mm^2, a compression area much larger than the compression regions created in our study. Hence, pressure effects on diffuse reflectance spectra could be very different. Reif, *et al.*, reported an

increase in μ_s' for *in vivo* mouse thigh muscle with increasing pressure, delivering a maximum pressure of 0.2 MPa [53]. The probe design used in Reif's study consisted of a flat tip close to 3 mm in diameter, similar to our probe tip design. Although our results showed an increase in μ_s' during the dwell period at the high strain condition (0.25 mm tissue thickness), we suspect that these results are due to geometrical limitations arising from our probe tip design, which will be discussed further. Lim, *et al.*, also reported an increase in scattering coefficient with increasing pressure on *in vivo* human forehead skin, applying a maximum pressure close to 0.15 MPa. Results in Lim's study varied depending on the type of tissue that was interrogated, mostly due to depth of vascularization in the tissue and the type of tissue (bony/fibrous/cellular) underlying the area interrogated [42].

Among the studies investigating probe pressure effects on diffuse reflectance spectroscopy, Chen, *et al.*, analyzed changes in spectra stemming from displacement-based compression in the near-infrared wavelength region [56]. They reported decreasing diffuse reflectance with increasing pressure between 1100 nm and 1700 nm. Diffuse reflectance intensity measurements were recorded from the palms of human subjects, and the compression procedure relied on subject feedback to determine when contact with the probe tip was established. This study employed the use of a pressure sensor, which allowed monitoring the pressure on the tissue while the probe was held at a fixed displacement. Although the study presented a displacement-based compression protocol, differences in pressure perception between human subjects (to determine at what position the probe tip contacted the skin) may have resulted in inconsistent calculation of the amount of tissue compression (strain). Conclusions in this study were based on pressure measurements. Additionally, their probe geometry consisted of concentric fiber bundles, with a central source optical fiber bundle and a peripheral detector optical fiber bundle. Source-detector bundle separation was close to 2.5 mm, which allowed interrogation up to 1 mm deep (dermis) for the wavelengths studied [60]. This probe design differs from the probe tip designs tested in our study, which could account for different effects on diffuse reflectance spectra. Furthermore, our robust compression procedure permitted repeatable tissue thickness conditions and resulted in a correlation between tissue strain, diffuse reflectance, and associated optical properties.

Chan, *et al.*, has previously reported a decrease in light transmission when mechanically compressing soft tissue [24]. This may have been due to the large area compression (~400 mm^2) that was used. The compression areas created in our study were significantly smaller than those

in Chan's study and demonstrated the diminishing returns on increasing compression area, with smaller changes in optical properties occurring with the larger probe tip area created by the 3 mm and 6 mm diameter hemispherical tips. We observed that the rate of light transmission increase during the dwell periods at constant tissue thickness correlated with the tissue load relaxation rate. This may suggest that during the dwell periods where thickness is held constant, the pressure gradient created during the compressive ramp drives interstitial fluid out of the zone of compression, creating a less turbid, optically cleared region. This can be seen in the increase in light transmission through the tissue in Figure 3-5. The effect was similar on the diffuse reflectance intensity. The magnitude of the pressure gradient created during compression (that drives interstitial fluid flow) correlates with the clearing effects observed in transmission experiments. Likewise, removal of fluid may result in a reduced index of refraction mismatch and therefore a lower scattering coefficient. We observed a dip in light transmission occurring during the ramp to reach the 0.25 mm tissue thickness condition (highest strain). This effect could be the result of competing mechanisms in optical clearing. As we have seen, changes in diffuse reflectance spectra are wavelength dependent, with a decrease in reflectance occurring at shorter wavelengths and an increase in reflectance occurring at longer wavelengths with greater compression. Thus, although the reflectance is increasing during the ramp and dwell periods, there may be an increase in the protein to water ratio during the ramp, which may reduce light transmission briefly until index of refraction mismatch is ultimately reduced by transient expulsion of water, allowing the light transmission to increase once again.

The acute change occurring when the thickness was held at 0.25 mm could be due to a number of factors. Compression of a soft, heterogeneous material such as skin redistributes constituents contained therein. High compression induced at this thickness condition (high strain) may cause light scatterers, such as cellular material and collagen fibers, to come closer to each other and behave optically as one bigger scatterer. This may cause a pronounced, monotonic increase in μ_s' during tissue relaxation as water moves out of the compressed region, due to the pressure gradient, and is replaced by highly scattering collagen fibers. Additionally, the redistribution of scatterers within the tissue causes the scattering length scales to be modified, further affecting the scattering at this thickness. The source-detector separation of 400 μm may also be playing a role in this effect. Since the tissue is only 250 μm thick at this point, the emitted photons may be interacting with the glass slide and reflective power meter sensor surface

underneath the tissue, introducing an alteration (possibly amplification) in the reflectance signal. Since this change was seen during the dwell period, we understand that there are coupled tissue clearing and probe geometry effects taking place. In order to better understand what was occurring during the dwell at high tissue strain, a simple experiment was designed. The reflectance signal of "thick" and "thin" *ex vivo* porcine skin specimens was evaluated to elucidate light interactions with the underlying material occurring due to the combination of probe source-detector separation and tissue thickness. Three different materials were placed underneath tissue specimens: a matte black paper, a glass slide, and a glass slide with the power meter sensor underneath (replicating the experimental setup used in our compression experiments). A schematic for the experimental setup with the matte black paper and the power meter sensor underneath the tissue specimen can be seen in Figure 3-12. The experimental setup for only the glass slide underneath the specimen was the same as Figure 3-12b, with the sensor removed.

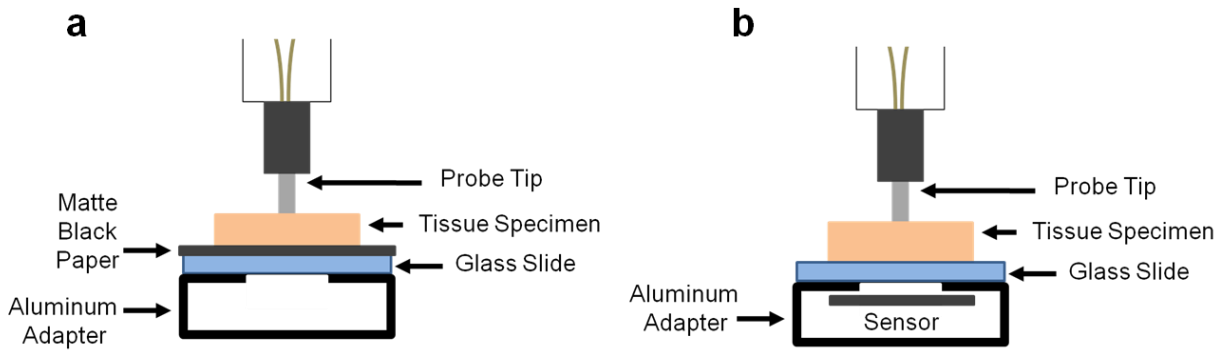

Figure 3-12: Schematic of experimental setup for different materials underneath the tissue specimens. (a) Matte black paper underneath tissue. (b) Sensor placed underneath glass slide and tissue.

The probe tip was brought into contact with the tissue specimen, defined as the position at which the magnitude of the load applied was 0.01 N, and a reflectance measurement was recorded. Three reflectance measurements were recorded for each specimen, one measurement for each underlying material condition. "Thick" specimens (N = 5) were 3 ± 0.4 mm thick, a thickness greater than the 400 μm source-detector separation. "Thin" specimens (N = 5) were 0.327 ± 0.03 mm thick, thinner than the probe's source-detector separation. As seen in Figure 3-13, the average reflectance for thick specimens was virtually equal for the three materials underneath the sample. Figure 3-14 shows the average reflectance for thin specimens.

Reflectance was highest when the sensor was present in the setup (similar to the experimental setup for the compression procedures), followed by only the glass slide underneath the sample, and finally the matte black paper. At this thickness condition, with our probe source-detector separation, light interacted with the materials underneath the tissue. Thus, the high strain condition in our compression study, when the tissue specimens were compressed to 0.25 mm, may have resulted in an artificially high reflectance (and associated optical properties).

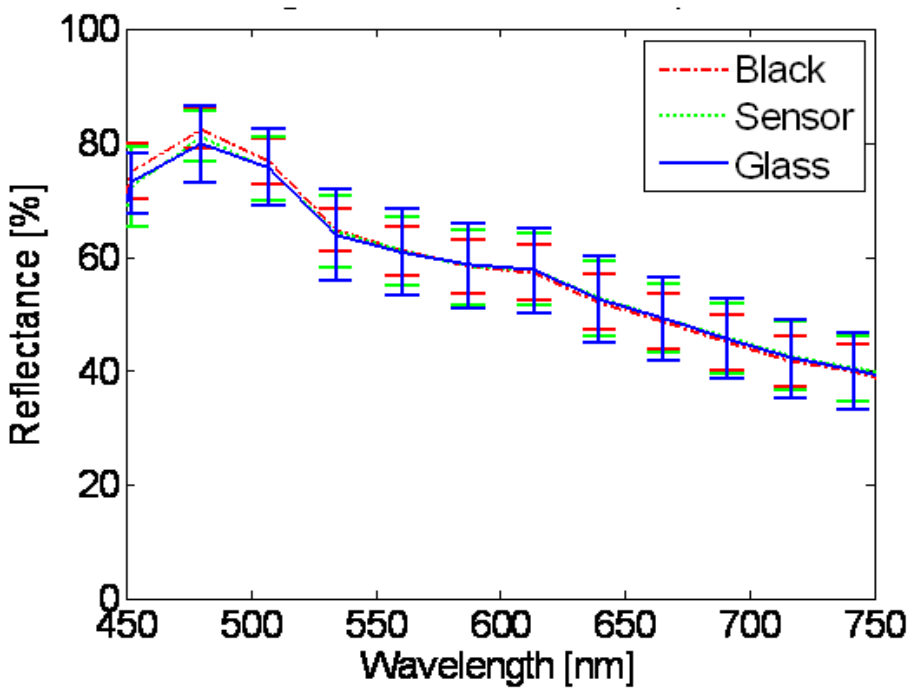

Figure 3-13: Average reflectance for thick specimens with three different underlying materials.

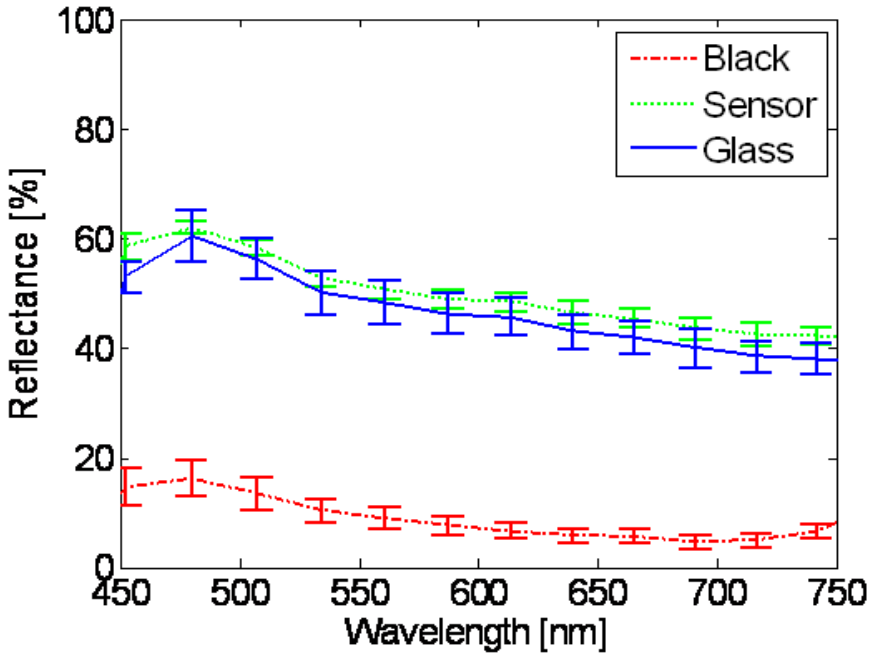

Figure 3-14: Average reflectance for thin specimens with three different underlying materials.

Tissue optical clearing studies have identified tissue dehydration (due to water displacement) as a potential mechanism for optical clearing [13-15, 17-21, 23, 26, 39]. Thus, we have investigated a technique that allows us to decouple changes in tissue thickness from interstitial fluid displacement (local dehydration) in order to monitor tissue optical property changes induced by the latter. It is understood that tissue thinning should contribute to changes in light transmission through tissue, reflectance, absorption, and tissue optical properties. However, our previous modeling study [40] has suggested that the contributions to changes in light transmission through tissue afforded by tissue thinning alone are not enough to match experimentally determined light transmission increases during localized compression.

3.5 Conclusion

We have provided the results of a systematic study of tissue optical clearing effects occurring during localized mechanical compression, using an isolated porcine skin model. By coupling a fiber based diffuse reflectance spectroscopy system to a mechanical load frame, we were able to collect dynamic diffuse reflectance spectra during displacement-controlled localized

compression of *ex vivo* porcine skin specimens. We also monitored simultaneous tissue thickness, load, and light transmission during the compression protocol. Our results indicate that localized compression causes changes in diffuse reflectance proportional to the amount of strain a tissue undergoes. Transient changes in reflectance were evident while tissue specimens were compressed and held at a constant thickness. At high strain, reflectance decreased at shorter wavelengths and increased at longer wavelengths. The rate of change in light transmission also correlated with the amount of strain experienced by the tissue. Transient changes in optical properties were observed, with greater reduction in reduced scattering coefficient occurring due to compression with hemispherical indenters and greater reduction in absorption coefficient occurring due to compression with a flat indenter. Our study results support the hypothesis that optical clearing effects due to localized mechanical compression are a coupled phenomenon of tissue thinning and altered optical properties. Changes in optical properties may be attributed to local tissue dehydration through lateral water expulsion and removal or redistribution of light absorbing chromophores. It is important to consider the contributions of other light scattering and absorbing chromophores, such as blood and melanin, to tissue optical properties. The effects of localized mechanical compression *in vivo* could differ from the results presented here due to the effects of blood perfusion, which is absent in this study. Thus, future work is necessary to more wholly quantify changes in optical properties due to mechanical compression using the technique described within this work *in vivo.* Based on our findings, localized mechanical compression allows modification of tissue optical properties, and may be harnessed as a minimally-invasive optical clearing technique to improve optical imaging, as well as provide additional advantages for light-based diagnostics, and laser-based therapeutics.

3.6 Acknowledgements

The authors would like to acknowledge the American Society for Lasers in Medicine and Surgery for a travel grant awarded to present research leading to this study at the 31st Annual ASLMS Conference in Grapevine, Texas during April 2011. Additionally, we thank the Virginia Tech Initiative to Maximize Student Diversity, funded by NIH Behavioral and Biomedical

Sciences and Engineering Research Training Grant R25 GM072767. William C. Vogt is supported by the Institute for Critical Technology and Applied Science (ICTAS) Doctoral Scholars Program at Virginia Tech. Finally, we would like to thank Mr. Matthias Hofmann for his help and guidance during probe construction.

Chapter 4: Conclusions, Future Work, and Applications

4.1 Conclusions

This research focused on interrelated studies that aim to discover the effects of localized mechanical compression on biological tissue optical properties. Chapter 2 describes the effects of localized mechanical compression as an "optical clearing" technique on image resolution and contrast of a target imaged through *ex vivo* biological tissue. Chapter 2 also presents a supplementary study investigating the thickness-independent effects of mechanical compression on light transmission through *ex vivo* biological tissue. Results indicate that employing this non-invasive mechanical clearing technique causes an increase in the ability to resolve a target image through biological tissue. Compared to conventional chemical clearing techniques, mechanical compression allowed visualization of targets ~4 times smaller with ~2 times higher contrast sensitivity. Higher tissue strain correlated with improved resolution and contrast sensitivity of the resolved image. Additionally, a transient increase in light transmission was reported without further tissue thinning. These results suggest that mechanical tissue optical clearing effects are due to both tissue thinning as well as an additional coupled mechanism, which may be local tissue dehydration.

Chapter 3 describes the effects of localized mechanical compression on the optical properties of *ex vivo* porcine skin specimens. The study aimed to reveal the dynamic changes in the scattering and absorption coefficients by monitoring tissue diffuse reflectance spectra during a displacement-controlled compression protocol. Differences in indenter geometry were also investigated. Results showed a reduction in scattering and absorption during compression with all indenters tested. A more monotonic, thickness independent reduction in scattering resulted when compressing the tissue with smaller surface area hemispherical indenters, whereas a more consistent reduction in absorption resulted from compression with the smallest surface area (flat tip) indenter. Nevertheless, an increase in both scattering and absorption occurred at high strain conditions, indicating that there are other effects that need to be investigated, achievable by possibly modifying our experimental setup or optical property extraction technique. Further work is needed to confirm whether the results are repeatable *in vivo*. Nevertheless, the strategy

presented yielded novel information about the thickness-independent optical clearing effects of localized mechanical compression in a controlled manner that could be easily replicated for *in vivo* studies.

4.2 Future Work

There are many variables, either directly related to the studies presented in this work, as well as to the field of tissue optical clearing in general, that may be addressed in future work. Doing so would provide a more complete, robust documentation of the effects, possible applications, and translational potential of mechanical tissue optical clearing.

4.2.1 In vivo Analysis of Localized Mechanical Compression Effects on Light Transmission

The majority of studies evaluating the effects of mechanical optical clearing through tissue have involved testing *ex vivo* tissue specimens. We understand that blood and interstitial fluid perfusion contribute greatly to native tissue optical properties and thus find it imperative to evaluate the effects of localized mechanical compression on light transmission *in vivo*. Though a complex endeavor, this analysis may be possible by preparing *in vivo* rodent specimens using a dorsal skinfold window chamber approach [64, 65]. This chamber allows observations across the full thickness of the skin and seems suitable for light transmission measurements during the application of localized mechanical compression *in vivo*. The experimental procedures detailed in Chapter 2 could be replicated, with modifications to overcome the added complexity of working with *in vivo* tissues. The procedure would allow simultaneous monitoring of light transmission, load, and tissue strain as well as subsequent imaging resolution and contrast assessment.

4.2.2 In vivo Analysis of Tissue Optical Properties during Localized Mechanical Compression

Evaluation of the effects of localized mechanical compression on tissue optical properties could be monitored *in vivo* using the dorsal skinfold chamber approach described in the previous section by implementing the diffuse reflectance spectroscopy techniques described in Chapter 3. Furthermore, with the appropriate Institutional Review Board approval, these experiments could be carried out on *in vivo* human skin. For this experimental procedure, the dorsal skinfold chamber would not be used and light transmission would not be monitored. However, diffuse

reflectance spectra would be monitored during the controlled application of localized mechanical compression, allowing the dynamic assessment of tissue optical clearing occurring due to compression. We expect the modification of tissue optical properties to be more pronounced, since the tissue will be perfused and the relative change in water/blood content before and after compression would be greater.

4.2.3 Histological Analysis of Localized Mechanical Compression Effects on Tissue

In vivo evaluation of the tissue optical clearing effects of localized mechanical compression should be followed by a histological analysis of the indented tissue. Previous studies have investigated the effects of long term localized compression on rodent muscle [66, 67]. Results showed reorganization of internal muscle fibers, cellular infiltration, localized inflammation, and even necrosis. These results were observed after lengthy (>2 hrs) indentation at high pressures, which is different from our shorter indentation technique. However, the effects of our localized mechanical compression technique should be evaluated histologically in order to determine injury threshold parameters and optimize this tissue optical clearing technique for potential clinical translation.

4.3 Potential Applications

Many potential applications may stem from the mechanical tissue optical clearing technique investigated in our studies. First and foremost, this technique may be used to improve light-based diagnostic, therapeutic, and cosmetic procedures. Tissue optical clearing devices, discussed earlier, may allow quick translation to research and clinical applications and are potentially easy and economical to manufacture. Given our observations on the transient changes in tissue optical properties during tissue relaxation, our mechanical compression technique may also be used to study the difference in transient response between healthy and diseased tissue. For example, neoplastic tissue is usually characterized as being highly vascularized, with higher water content than normal [68]. The lateral expulsion of water and blood that we hypothesize occurs during localized mechanical compression may be different between healthy and neoplastic tissue, and may correlate to the disease state of the tissue. Thus, monitoring the dynamics of tissue optical property change during tissue relaxation after localized mechanical compression could be used to

differentiate between healthy and neoplastic tissue, especially useful in defining the margins of tumors fated for excision. Finally, the changes in diffuse reflectance spectra occurring due to tissue compression could be used as a pressure sensing parameter for pressure sensitive probing applications. Tissue optical clearing and its applications holds broad potential for light-based clinical and diagnostic procedures.

4.4 Concluding Remarks

The potential benefits and broad applications of mechanical compression as a tissue optical clearing techniques have not been fully explored. However, this research addresses a major aspect of the techniques potential by being the first to systematically evaluate the effects of localized compression on image recovery, resolution and contrast, light transmission enhancement, and modification of tissue optical properties. The results obtained from this research indicate this technique may prove useful in imaging, diagnostic, therapeutic, and cosmetic applications.

References

1. Edwards, C. and R. Marks, *Evaluation of biomechanical properties of human skin.* Clinics in Dermatology, 1995. **13**(4): p. 375-380.
2. Oomens, C.W.J., D.H. Vancampen, and H.J. Grootenboer, *A MIXTURE APPROACH TO THE MECHANICS OF SKIN.* Journal of Biomechanics, 1987. **20**(9): p. 877-885.
3. Welch, A.J. and M.J.C.v. Gemert, *Optical-thermal response of laser-irradiated tissue*. Lasers, photonics, and electro-optics1995, New York: Plenum Press. xxvi, 925 p.
4. Delalleau, A., et al., *A nonlinear elastic behavior to identify the mechanical parameters of human skin in vivo.* Skin Research and Technology, 2008. **14**(2): p. 152-164.
5. Wang, X., M.C. Chang, and J.S. Nelson, *Group refractive index measurement of dry and hydrated journal article I collagen films using optical low-coherence reflectometry*. Vol. 1. 1996: SPIE. 212-216.
6. Brunsting, A. and P.F. Mullaney, *DIFFERENTIAL LIGHT SCATTERING FROM SPHERICAL MAMMALIAN CELLS.* Biophysical Journal, 1974. **14**(6): p. 439-453.
7. Schmitt, J.M. and G. Kumar, *Optical scattering properties of soft tissue: a discrete particle model.* Applied Optics, 1998. **37**(13): p. 2788-2797.
8. Fercher, A.F., *Optical coherence tomography - development, principles, applications.* Z Med Phys, 2010. **20**(4): p. 251-76.
9. Carlson, A.L., et al., *Dual-mode reflectance and fluorescence near-video-rate confocal microscope for architectural, morphological and molecular imaging of tissue.* Journal of Microscopy-Oxford, 2007. **228**(1): p. 11-24.
10. Pavlova, I., et al., *Microanatomical and biochemical origins of normal and precancerous cervical autofluorescence using laser-scanning fluorescence confocal microscopy.* Photochemistry and Photobiology, 2003. **77**(5): p. 550-555.
11. Wang, G., et al., *Overview of bioluminescence tomography-a new molecular imaging modality.* Frontiers in Bioscience, 2008. **13**: p. 1281-1293.
12. Liu, H., et al., *Dependence of tissue optical properties on solute-induced changes in refractive index and osmolarity.* Journal of biomedical optics, 1996. **1**(2): p. 200-211.
13. Choi, B., et al., *Determination of chemical agent optical clearing potential using in vitro human skin.* Lasers in surgery and medicine, 2005. **36**(2): p. 72-75.
14. Kang, H., et al., *Evaluation of laser beam profile in soft tissue due to compression, glycerol, and micro-needling.* Lasers in surgery and medicine, 2008. **40**(8): p. 570-575.
15. Rylander, C.G., et al., *Dehydration mechanism of optical clearing in tissue.* Journal of biomedical optics, 2006. **11**(4).
16. Samatham, R., K.G. Phillips, and S.L. Jacques, *Assessment of optical clearing agents using reflectance-mode confocal scanning laser microscopy.* J Innov Opt Health Sci, 2010. **3**(3): p. 6.
17. Tuchin, V.V., et al., *Light propagation in tissues with controlled optical properties.* Journal of biomedical optics, 1997. **2**(4): p. 401-417.
18. Vargas, G., et al., *Use of osmotically active agents to alter optical properties of tissue: Effects on the detected fluorescence signal measured through skin.* Lasers in surgery and medicine, 2001. **29**(3): p. 213-220.
19. Vargas, O., et al., *Use of an agent to reduce scattering in skin.* Lasers in surgery and medicine, 1999. **24**(2): p. 133-141.

20. Yeh, A.T., et al., *Reversible dissociation of collagen in tissues.* Journal of Investigative Dermatology, 2003. **121**(6): p. 1332-1335.
21. Rylander, C.G., et al., *Mechanical tissue optical clearing devices: Enhancement of light penetration in ex vivo porcine skin and adipose tissue.* Lasers in Surgery and Medicine, 2008. **40**(10): p. 688-694.
22. Izquierdo-Roman, A., W. Vogt, and C. Rylander, *MECHANICAL TISSUE OPTICAL CLEARING TECHNIQUE INCREASES RESOLUTION AND CONTRAST OF A TARGET IMAGE BENEATH EX VIVO PORCINE SKIN.* Lasers in surgery and medicine, 2011. **43**: p. 914-914.
23. Drew, C., T.E. Milner, and C.G. Rylander, *Mechanical tissue optical clearing devices: evaluation of enhanced light penetration in skin using optical coherence tomography.* Journal of biomedical optics, 2009. **14**(6): p. 064019.
24. Chan, E.K., et al., *Effects of compression on soft tissue optical properties.* Ieee Journal of Selected Topics in Quantum Electronics, 1996. **2**(4): p. 943-950.
25. Sung, K.B., et al., *Near real time in vivo fibre optic confocal microscopy: sub-cellular structure resolved.* Journal of Microscopy-Oxford, 2002. **207**: p. 137-145.
26. Khan, M.H., et al., *Optical clearing of in vivo human skin: implications for light-based diagnostic imaging and therapeutics.* Lasers in surgery and medicine, 2004. **34**(2): p. 83-5.
27. Fischer, A.A., *PRESSURE TOLERANCE OVER MUSCLES AND BONES IN NORMAL SUBJECTS.* Archives of Physical Medicine and Rehabilitation, 1986. **67**(6): p. 406-409.
28. Lee, W.C., M. Zhang, and A.F. Mak, *Regional differences in pain threshold and tolerance of the transtibial residual limb: Including the effects of age and interface material.* Archives of Physical Medicine and Rehabilitation, 2005. **86**(4): p. 641-649.
29. Pickering, G., et al., *Impact of age, gender and cognitive functioning on pain perception.* Gerontology, 2002. **48**(2): p. 112-118.
30. Xiong, S.P., et al., *An indentation apparatus for evaluating discomfort and pain thresholds in conjunction with mechanical properties of foot tissue in vivo.* Journal of Rehabilitation Research and Development, 2010. **47**(7): p. 629-641.
31. Goncalves, D.P. and D.J. Griffith, *Estimating uncertainty in resolution tests.* Optical Engineering, 2006. **45**(5).
32. Hecht, E., *Optics*2002, San Francisco: Addison Wesley. 688.
33. Levenson, E., P. Lerch, and M.C. Martin, *Infrared imaging: Synchrotrons vs. arrays, resolution vs. speed.* Infrared Physics & Technology, 2006. **49**(1-2): p. 45-52.
34. Kelly, D.H., *Spatial Frequency, Bandwidth, and Resolution.* Appl. Opt., 1965. **4**(4): p. 435-435.
35. Zuzak, K.J., et al., *Visible reflectance hyperspectral imaging: Characterization of a noninvasive, in vivo system for determining tissue perfusion.* Analytical Chemistry, 2002. **74**(9): p. 2021-2028.
36. Atencio, J.A.D. and et al., *Influence of probe pressure on human skin diffuse reflectance spectroscopy measurements.* Optical Memory and Neural Networks, 2009. **18**(1): p. 6.
37. Ti, Y. and W.-C. Lin, *Effects of probe contact pressure on in vivo optical spectroscopy.* Opt. Express, 2008. **16**(6): p. 4250-4262.
38. Rachel Estelle, T. and et al., *Improved depth resolution in near-infrared diffuse reflectance spectroscopy using obliquely oriented fibers.* Journal of biomedical optics, 2009. **14**(2): p. 024026.

39. Wang, R.K.K., et al., *Concurrent enhancement of imaging depth and contrast for optical coherence tomography by hyperosmotic agents.* Journal of the Optical Society of America B-Optical Physics, 2001. **18**(7): p. 948-953.
40. Vogt, W.C., et al., *Parametric Study of Tissue Optical Clearing by Localized Mechanical Compression using Combined Finite Element and Monte Carlo Simulation.* J Innov Opt Health Sci, 2010. **3**(3): p. 9.
41. Bigio, I.J. and S.G. Bown, *Spectroscopic sensing of cancer and cancer therapy - Current status of translational research.* Cancer Biology & Therapy, 2004. **3**(3): p. 259-267.
42. Lim, L.A., et al., *Probe pressure effects on human skin diffuse reflectance and fluorescence spectroscopy measurements.* Journal of biomedical optics, 2011. **16**(1).
43. Rajaram, N., et al., *Design and validation of a clinical instrument for spectral diagnosis of cutaneous malignancy.* Applied Optics, 2010. **49**(2): p. 142-152.
44. Rajaram, N., T.H. Nguyen, and J.W. Tunnell, *Lookup table-based inverse model for determining optical properties of turbid media.* Journal of biomedical optics, 2008. **13**(5).
45. Farrell, T.J., M.S. Patterson, and B. Wilson, *A DIFFUSION-THEORY MODEL OF SPATIALLY RESOLVED, STEADY-STATE DIFFUSE REFLECTANCE FOR THE NONINVASIVE DETERMINATION OF TISSUE OPTICAL-PROPERTIES INVIVO.* Medical Physics, 1992. **19**(4): p. 879-888.
46. Mourant, J.R., et al., *Predictions and measurements of scattering and absorption over broad wavelength ranges in tissue phantoms.* Applied Optics, 1997. **36**(4): p. 949-957.
47. Zonios, G., et al., *Diffuse reflectance spectroscopy of human adenomatous colon polyps in vivo.* Applied Optics, 1999. **38**(31): p. 6628-6637.
48. Brown, J.Q., et al., *Advances in quantitative UV-visible spectroscopy for clinical and pre-clinical application in cancer.* Current Opinion in Biotechnology, 2009. **20**(1): p. 119-131.
49. Vishwanath, K., et al., *Portable, Fiber-Based, Diffuse Reflection Spectroscopy (DRS) Systems for Estimating Tissue Optical Properties.* Applied Spectroscopy, 2011. **65**(2): p. 206-215.
50. Amelink, A., et al., *In vivo measurement of the local optical properties of tissue by use of differential path-length spectroscopy.* Optics Letters, 2004. **29**(10): p. 1087-1089.
51. Lovat, L.B., et al., *Elastic scattering spectroscopy accurately detects high grade dysplasia and cancer in Barrett's oesophagus.* Gut, 2006. **55**(8): p. 1078-1083.
52. Mirabal, Y.N., et al., *Reflectance spectroscopy for in vivo detection of cervical precancer.* Journal of biomedical optics, 2002. **7**(4): p. 587-594.
53. Reif, R., et al., *Analysis of changes in reflectance measurements on biological tissues subjected to different probe pressures.* Journal of biomedical optics, 2008. **13**(1).
54. Zonios, G. and A. Dimou, *Modeling diffuse reflectance from semi-infinite turbid media: application to the study of skin optical properties.* Optics Express, 2006. **14**(19): p. 8661-8674.
55. Bigio, I.J., O. A. amar, and M.S. Hirsch. *Elastic scattering spectroscopy for detection of prostate cancer: preliminary feasibility study*. 2003. Optical Society of America.
56. Chen, W.L., et al., *Influence of contact state on NIR diffuse reflectance spectroscopy in vivo.* Journal of Physics D-Applied Physics, 2005. **38**(15): p. 2691-2695.
57. Murphy, B.W., et al., *Toward the discrimination of early melanoma from common and dysplastic nevus using fiber optic diffuse reflectance spectroscopy.* Journal of biomedical optics, 2005. **10**(6).

58. Nath, A., et al., *Effect of probe pressure on cervical fluorescence spectroscopy measurements.* Journal of biomedical optics, 2004. **9**(3): p. 523-533.
59. Ruderman, S., et al., *Analysis of pressure, angle and temporal effects on tissue optical properties from polarization-gated spectroscopic probe measurements.* Biomed. Opt. Express, 2010. **1**(2): p. 489-499.
60. Chen, W., et al., *Application of transcutaneous diffuse reflectance spectroscopy in the measurement of blood glucose concentration.* Chin. Opt. Lett., 2004. **2**(7): p. 411-410.
61. Izquierdo-Roman, A. and C. Rylander, *MEASUREMENT OF INCREASED LIGHT TRANSMISSION AND STRAIN AS A FUNCTION OF MECHANICAL COMPRESSION IN EX VIVO PORCINE SKIN.* Lasers in surgery and medicine, 2010: p. 9-9.
62. Izquierdo-Roman, A., et al., *Mechanical Tissue Optical Clearing Technique Increases Imaging Resolution and Contrast through Ex Vivo Porcine Skin.* Lasers in Surgery and Medicine, *In Press*.
63. Meglinsky, I. and S. Matcher, *Modelling the sampling volume for skin blood oxygenation measurements.* Medical and Biological Engineering and Computing, 2001. **39**(1): p. 44-50.
64. Papenfuss, H.D., et al., *A transparent access chamber for the rat dorsal skin fold.* Microvascular research, 1979. **18**(3): p. 311-8.
65. Sckell, A. and M. Leunig, *The Dorsal Skinfold Chamber: Studying Angiogenesis by Intravital Microscopy*, 2008. p. 305-317.
66. Linder-Ganz, E. and A. Gefen, *Mechanical compression-induced pressure sores in rat hindlimb: muscle stiffness, histology, and computational models.* Journal of Applied Physiology, 2004. **96**(6): p. 2034-2049.
67. Stekelenburg, A., et al., *Compression-induced deep tissue injury examined with magnetic resonance imaging and histology.* Journal of Applied Physiology, 2006. **100**(6): p. 1946-1954.
68. Kiricuta, I.C. and V. Simplaceanu, *TISSUE WATER-CONTENT AND NUCLEAR MAGNETIC-RESONANCE IN NORMAL AND TUMOR TISSUES.* Cancer Research, 1975. **35**(5): p. 1164-1167.

Appendix A: Annotated List of Figures

Appendix B: Copyright Permission Letter

Alondra Izquierdo-Roman <aizquie@gmail.com>

LSM Article in Proofing

2 mensajes

Alondra Izquierdo-Roman <aizquie@gmail.com> **1 de agosto de 2011 15:44**

Para: PermissionsUS@wiley.com

Hi,

I am trying to obtain permission to use a manuscript that has been accepted for publication by Lasers in Surgery and Medicine (and is in the proofing stage) as part of my master's thesis. I understand that this is something that is done frequently, and the graduate school at my university requires documentation of permission from the publishers in order to approve my thesis. I believe an e-mail communication is sufficient. The manuscript ID, as per LSM's system, is LSM-10-0286.R2. The manuscript is entitled: Mechanical Tissue Optical Clearing Technique Increases Imaging Resolution and Contrast through Ex Vivo Porcine Skin.

Please advise. I appreciate all the help :)

Sincerely,

Alondra Izquierdo-Roman

--

'With hurricanes, tornadoes, fires out of control, mud slides, flooding, severe thunderstorms tearing up the country from one end to another, and with the threat of bird flu and terrorist attacks, are we sure this is a good time to take God out of the Pledge of Allegiance?'

Permissions - US <permissionsus@wiley.com> **2 de agosto de 2011 09:12**

Para: Alondra Izquierdo-Roman <aizquie@gmail.com>

Dear Alondra:

Thank you for your request. John Wiley & Sons, Inc. has no objections to your proposed reuse of this material.

Permission is hereby granted for the use requested subject to the usual acknowledgements (title, volume number, issue number, year, page numbers. Copyright [year and owner]. And the statement "This material is reproduced with permission of John Wiley & Sons, Inc."). Any third party material is expressly excluded from this permission. If any of the material you wish to use appears within our work with credit to another source, authorization from that source must be obtained. This permission does not include the right to grant others permission to photocopy or otherwise reproduce this material except for versions made by non-profit organizations for use by the blind or handicapped persons.

Best wishes,

Paulette Goldweber

Associate Manager, Permissions

Global Rights

John Wiley & Sons, Inc.

ph: 201-748-8765

f: 201-748-6008

pgoldweb@wiley.com